National Library of Canada
Bibliothèque nationale du Canada

Canadian Theses Service
Service des thèses canadiennes

Ottawa, Canada
K1A 0N4

NOTICE

The quality of this microform is heavily dependent upon the quality of the original thesis submitted for microfilming. Every effort has been made to ensure the highest quality of reproduction possible.

If pages are missing, contact the university which granted the degree.

Some pages may have indistinct print especially if the original pages were typed with a poor typewriter ribbon or if the university sent us an inferior photocopy.

Reproduction in full or in part of this microform is governed by the Canadian Copyright Act, R.S.C. 1970, c. C-30, and subsequent amendments.

AVIS

La qualité de cette microforme dépend grandement de la qualité de la thèse soumise au microfilmage. Nous avons tout fait pour assurer une qualité supérieure de reproduction.

S'il manque des pages, veuillez communiquer avec l'université qui a conféré le grade.

La qualité d'impression de certaines pages peut laisser à désirer, surtout si les pages originales ont été dactylographiées à l'aide d'un ruban usé ou si l'université nous a fait parvenir une photocopie de qualité inférieure.

La reproduction, même partielle, de cette microforme est soumise à la Loi canadienne sur le droit d'auteur, SRC 1970, c. C-30, et ses amendements subséquents.

NL-339 (r. 88/04) c

Canada

UNIVERSITY OF ALBERTA

VERTICAL VELOCITY FIELDS IN A DIABATICALLY FORCED MESOSCALE CIRCULATION: A NUMERICAL STUDY.

BY

OLE JACOBSEN

A thesis submitted to the Faculty of Graduate Studies and Research in partial fulfilment of the requirements for the degree of Master of Science.

IN

Meteorology

DEPARTMENT OF GEOGRAPHY

Edmonton, Alberta
Spring 1992

National Library of Canada
Bibliothèque nationale du Canada

Canadian Theses Service
Service des thèses canadiennes

Ottawa, Canada
K1A 0N4

The author has granted an irrevocable non-exclusive licence allowing the National Library of Canada to reproduce, loan, distribute or sell copies of his/her thesis by any means and in any form or format, making this thesis available to interested persons.

The author retains ownership of the copyright in his/her thesis. Neither the thesis nor substantial extracts from it may be printed or otherwise reproduced without his/her permission.

L'auteur a accordé une licence irrévocable et non exclusive permettant à la Bibliothèque nationale du Canada de reproduire, prêter, distribuer ou vendre des copies de sa thèse de quelque manière et sous quelque forme que ce soit pour mettre des exemplaires de cette thèse à la disposition des personnes intéressées.

L'auteur conserve la propriété du droit d'auteur qui protège sa thèse. Ni la thèse ni des extraits substantiels de celle-ci ne doivent être imprimés ou autrement reproduits sans son autorisation.

ISBN 0-315-73120-6

Canada

UNIVERSITY OF ALBERTA

RELEASE FORM

NAME OF AUTHOR: OLE JACOBSEN

TITLE OF THESIS: VERTICAL VELOCITY FIELDS IN A DIABATICALLY FORCED MESOSCALE CIRCULATION: A NUMERICAL STUDY.

DEGREE: MASTER OF SCIENCE

YEAR THIS DEGREE GRANTED: SPRING 1992

Permission is hereby granted to the University of Alberta Library to reproduce single copies of this thesis and to lend or sell such copies for private, scholarly or scientific research purposes only.

The author reserves all other publication and other rights in association with the copyright in the thesis, and except as hereinbefore provided neither the thesis nor any substantial portion thereof may be printed or otherwise reproduced in any material form whatever without the author's prior written permission.

Ole Jacobsen
5 Meredian Rd
Sherwood Park AB
T8A 0N5

Apr 10, 1992

UNIVERSITY OF ALBERTA

FACULTY OF GRADUATE STUDIES AND RESEARCH

The undersigned certify that they have read, and recommend to the Faculty of Graduate Studies and Research for acceptance, a thesis entitled 'VERTICAL VELOCITY FIELDS IN A DIABATICALLY FORCED MESOSCALE CIRCULATION: A NUMERICAL STUDY.' submitted by Ole Jacobsen in partial fulfilment of the requirements for the degree of Master of Meteorology.

G. Reuter

G. Reuter

J.D. Wilson

J.D. Wilson

G.E. Swaters

G.E. Swaters

April 1992

DEDICATION

This thesis is dedicated to those who gave their support and love during the period required to complete this work; Linda, Kyla, Michael and Emily.

ABSTRACT

The effects of various atmospheric conditions on the vertical motion field in a diabatically forced mesoscale circulation are investigated. We use a "buoyancy wave" model based on linearized steady state equations governing a stably stratified sheared airflow with an elevated diabatic heating source that moves with the mean flow. Friction is approximated using a momentum sink linear in the velocity. Both slab axisymmetric and symmetric heating sources are considered, leading to two and three dimensional simulations.

A series of model experiments quantify the sensitivity of the vertical motion field to the heating source, the thermal stratification, the dissipation rate and various profiles of the ambient wind. Profiles included are constant wind shear, parabolic wind profiles, low level jet profiles and directional shear cases. The results show that certain model parameters effect the vertical motion fields by enhancing the updraft speeds or by changing the structure (i.e. the tilt of the updraft core). Our major findings are:

1) An increase in the magnitude of the shear increases the speed of the peak updraft. Furthermore, it also increases the upwind tilt of the updraft core in the lower troposphere. On the other hand, an increase in wind shear decreases the downwind tilt in the secondary updraft in the upper troposphere.

2) An increase in the static stability (i.e. decrease in the Brunt-Väisälä frequency) causes a significant increase in the speed of the peak updraft. Also the circulation becomes more erect.

3) An increase in the magnitude of the dissipation coefficient, decreases the intensity of the circulation and also makes the circulation more erect.

4) The magnitude of the maximum vertical velocity increases when the curvature (i.e. second derivative) of the ambient wind decreases provided the first derivative remains positive throughout the heating layer.

5) An increase in the diabatic heating rate, increases the strength of the vertical motion field.

6) Increasing the depth of the diabatic heating source, makes the circulation more erect.

7) When the wavenumber of the heating and the Scorer parameter (which is a function of the static stability, the ambient wind and the second derivative of the wind) are similar, the updraft field becomes organized and very intense.

8) A low level jet with a maximum speed opposite in direction to the flow aloft contributes to convective activity due to enhanced buoyancy waves.

9) The model results are consistent with observations for the Alberta storm of 3 July 1991.

ACKNOWLEDGEMENT

Special thanks to Gerhard my supervisor and cross-hall neighbour who endured innumerable questions and always found the time to find the answer.

Special thanks to my parents (Frits and Elsabeth) for giving me confidence in my abilities.

I would like to thank Atmospheric Environment Services for their financial support and their belief in my abilities.

Table of Contents

	Page
1. Introduction	1
1.1 Storm development and wind shear	1
1.2 Approach	4
1.3 Organization of Thesis	6
2. Model Formulation and Numerical Model	8
2.1 Basic assumptions	8
2.2 Equations of motion	9
2.3 Numerical method	11
2.4 Slab symmetry	12
3. Interpretation of the Analytical Solution and the Scorer Parameter	16
3.1 Analytic solution without dissipation	16
3.2 Analytical solution with dissipation	19
4. Model Parameters and Sensitivity	21
4.1 Control Case	21
4.2 Model sensitivity	26
4.3 Discussion	35
5. Changes in the Vertical Motion Fields due to Wind Shear	37
5.1 Vertical stratification of static stability	37
5.2 Constant shear of the ambient wind	38
5.3 Second derivative of the ambient wind	41
5.4 Low level jet streams	46
5.5 The Scorer Parameter	52
6. Three Dimensional Model Results	56
6.1 3-D model with a slab-symmetric heating structure	56
6.2 3d model results with a three-dimensional heating source	58
6.3 Effects of the change of wind direction	60
7. Case Study	64
8. Discussion and Conclusions	70
9. References	75
Appendix 1	79
Appendix 2	81

List of Tables

Table		Page
4.1	Summary of sensitivity tests	27
5.2.1	Comparison of the vertical motion field associated with various constant wind shear profiles	39
5.3	Comparison of the vertical motion field associated with various constant second derivatives of the horizontal wind	43
5.4.1	Comparison of the vertical velocities and kinetic energies associated with low level jets	48
5.4.2	Comparison of the kinetic energy and the maximum vertical velocity associated with a classification 2 low level jet with different static stability	51
5.4.3	Kinetic energy and maximum vertical velocity associated with a classification 1 low level jet defined in a moving frame of reference	51
5.5	Comparison of vertical velocities and kinetic energy associated with wind profiles calculated to achieve the strongest vertical motion field	55
6.2.1	Comparison of the vertical velocities and kinetic energies associated with a single cell in various uni-directional constant shears	60
6.3.1	Vertical velocities and kinetic energies associated with directional shear	61
7.1	Comparison of peak vertical velocities and kinetic energies associated with case study	66

List of Figures

Figure		Page
4.1.1	Control case basic state wind	22
4.1.2	Heating rate for control case	24
4.1.3	Control case potential temperature profile	25
4.1.4	Control case vertical motion field	25
4.2.1	Magnitude of the diabatic heating rate and corresponding vertical motion fields	28
4.2.2	Depth of the diabatic heating rate and corresponding vertical motion fields	29
4.2.3	Vertical velocity field as the speed of the heat source is changed	31
4.2.4	Comparison of the vertical velocity field using different values for the coefficient of Rayleigh friction and Newtonian Cooling	32
4.2.5	Vertical motion fields for N = .0094 s^{-1} and N = .0124 s^{-1}	33
4.2.6	Vertical motion fields associated with constant shears	34
5.1.1	Potential temperature profile	37
5.2.1	Wind profiles (constant shear) and corresponding vertical motion fields	40
5.3.1	Wind profiles (non-constant shear) and corresponding vertical motion fields	42
5.3.2	Wind profiles (non-constant shear in heated layer) and corresponding vertical motion fields	45
5.3.3	Intensity of the vertical motion field associated with various second derivatives of the wind	46
5.4.1	Low level jets with associated vertical motion fields	49

Figure		Page
5.4.2	Vertical motion field associated with a classification 2 low level jet in a destabilized environment	50
5.4.3	Wind profile and vertical motion field. Wind profile is a classification 1 low level jet in a moving frame of reference	52
5.5.1	Wind profile associated with maximum enhancement of the vertical motion field	53
5.5.2	Vertical motion field using wind profile derived from Scorer parameter to achieve maximum enhancement	54
5.5.3	Estimated effective wind in a moving frame of reference to achieve maximum enhancement of the vertical motion field	54
6.1.1	Comparison of the three dimensional case to the two dimensional case	57
6.1.2	Vertical motion field associated with the wind parallel to the gradient of heating	57
6.2.1	Three dimensional vertical motion fields for a "bubble like" heating source and constant shear	59
6.3.1	V component of the ambient wind	61
6.3.2	Vertical velocity fields for three dimensional "bubble like cell" in a directionally sheared environment	62
6.3.3	Horizontal section of vertical motion fields associated with different V-component of wind	63
7.1	Average potential temperature profile for July 3, 1991	64
7.2	Morning and afternoon horizontal wind components	65
7.3	Vertical motion fields for case study	67
7.4	Horizontal section of vertical motion fields	68

List of Symbols

U	basic state velocity in the x-direction
V	basic state velocity in the y-direction
ρ	basic state density
T	basic state temperature: tropopause
N	Brunt-Väisälä frequency
u	perturbation velocity in the x-direction
v	perturbation velocity in the y-direction
w	vertical velocity in the z-direction
P	perturbation pressure
ϱ	perturbation density
C	specific heat capacity at constant pressure
β	coefficient of Rayleigh friction and Newtonian cooling
q	diabatic heating rate
B	half-width of the heating term
h	base of the heating term
H	top of the heating term
g	acceleration due to gravity
D	top of the model atmosphere
k	wave number in x-direction
l	wave number in y-direction

1 Introduction

1.1 Storm development and wind shear

Upward vertical motion drives a convective storm. The expansion of the ascending air causes substantial cooling which often results in condensation of water vapour and the formation of clouds. The condensation releases latent heat which provides the energy to strengthen the buoyancy and storm updraft. Thus, the storm updraft is largely regulated by positive feedback processes involving diabatic heating. There is a need to expand our understanding of atmospheric conditions that favour the formation of storms.

How does the vertical shear of the ambient wind effect the organization, size and intensity of a convective storm? This question has intrigued researchers for the last few decades. Early observations (e.g. Byers and Braham 1949) suggested the growth of small and moderate size cumuli was suppressed by shear; in fact clouds were observed to be torn apart if the shear was too strong. The inhibiting effects due to the ambient wind shear on small to moderate size cumuli results from the displacement of the centre of maximum buoyancy relative to the maximum updraft (Steiner 1973).

The ambient wind shear can not only diminish the development of convective clouds and their life cycle (e.g. Pastushkov 1975) but may promote development for large rain-producing clouds. The large cumuli are enhanced by the

out of the updraft core, freeing it from the effects of precipitation drag and evaporative cooling below the cloud base. Outside the updraft core, the precipitation induced downdrafts enhance the sub-cloud convergence, producing a long-lasting circulation (Takeda 1971).

Estimates based on a form of the Bernoulli-equation suggest that the storm characteristics are regulated by the interaction of the available potential buoyant energy (APBE) and the ambient wind shear (e.g. Moncrieff and Green 1972). Weisman and Klemp (1982) used a three dimensional cloud model to investigate how storm intensity depends on the environmental Bulk Richardson Number, which is a measure of the ratio of the buoyancy and the mean wind shear. They found that for a given amount of APBE, weak wind shear produced short-lived single cells; moderate wind shear produces secondary cell development (similar to multicell storms); and strong wind shear together with low level veering produces an intense long lasting storm.

There is evidence that not only the gross shear between the surface and 50 kPa level is important, but also the detail of the profile. Numerical simulation have indicated that the storm structure depends largely on the amount of shear in the lowest 3 km and much less on the shear aloft (Wilhelmson and Klemp 1978). Others have found that a reversal of the shear can strongly affect the circulation pattern (Takeda 1971, Reuter and Yau 1987). Veering combined with strong wind shear produces a quasi-steady rotating updraft, characteristics for the so-called supercell storm (Wilhelmson and Klemp 1981). These findings from numerical cloud models agree well with typical hodographs for single cell, multicell and supercell storm observed during the Alberta Hail Studies project (Chrisholm and English 1973).

Although observed wind patterns seldom fit the idealized uni-directional structure, there is considerable theoretical interest in the uni-directional sheared storm environment. Uni-directional shear produces a highly asymmetric organization. The upwind portion of the storm are wetter and warmer than their downshear sides (e.g. Reuter and Yau 1987). Furthermore, downdrafts are typically formed at the downshear edge. The updraft seem to act as an obstacle to the wind, forcing the flow around the upshear portion of the circulation, protecting that region from entrainment, while the downshear portion experiences enhanced mixing. It is important that we understand the effects of the detail of uni-directional shear before examining the effects of directional shear, since, the interpretation of results for uni-directional shear is normally less complex.

Theoretical studies are clearly needed to help interpret the vast amounts of new data that will become available in the next decade. The ongoing revolution in the methods of collecting and managing atmospheric data will result in observations at a better temporal and spatial resolution. Instruments such as Doppler radar and wind profilers provide measurements of wind direction and speed at intervals of about twenty minutes. As this network becomes denser, the problem of using this data more effectively becomes increasingly important. Estimated temperature and moisture fields are becoming available on a finer grid due to better utilization of satellite data.

A numerical modelling studies simulating the interaction between the wind, diabatic heating and atmospheric stability to show that there exist combinations

of these parameters which provides an environment where storm development is enhanced. The wind profiles are examined in terms of the effects of the first and second derivative of the wind profile and low level jet streams on the circulation pattern.

1.2 Approach

To investigate how the vertical motion field is enhanced by atmospheric conditions there are essentially two different approaches: observation and numerical modelling. Since it is extremely difficult to measure directly the vertical motion field, we have adopted the numerical approach. The major advantage of this approach is that it allows us to examine the relative contribution of individual parameters on the enhancement of the circulation.

Uccellini et al (1987) used a detailed numerical model (Kaplan et al 1982) that simulated realistically a mesoscale circulation driven by diabatic heating. They concluded that there was a synergistic interaction between dynamic processes associated with jet streams. However, it was impossible to identify the exact mechanism that led to the intense interaction between low level and upper level processes. This suggests that a simpler model may facilitate the identification of the mechanisms that yield an enhanced circulation. A simple formulation of a diabatically driven circulation in a sheared environment is based on a steady-state linearized model using a wave-type solution. We will first discuss some of the concepts and studies associated with the buoyancy wave solution.

Buoyancy waves or gravity waves are defined to exist in a stably stratified atmosphere such that a fluid parcel

displaced vertically will undergo buoyancy oscillations (Gossard and Hooke 1975). The study of waves internal to the atmosphere was stimulated by the wave like appearance of clouds in the atmosphere. This has been verified by satellite images and pictures taken from aircraft. Recent observations by doppler radar indicated that the amplitude of the gravity waves is typically a factor of two larger in cloudy skies than clear skies (Nastrum et al 1990). Additionally, they reported an increase in gravity wave activity in association with low stability in the lower troposphere and with jet streams. These findings indicate that gravity or buoyancy wave activity increases substantially in the presence of clouds (latent heat release), in the presence of an upper level jet and in association with atmospheric stability. Since these are often the condition under which significant convection occurs it would be reasonable to assume that the interaction between these fields is linked by buoyancy waves.

Buoyancy wave solutions to the equations of motion have been used to model the effects of wind profiles and diabatic heating on vertical velocities. Raymond (1986) used a model based on the buoyancy wave solution, to show that the low level jet appears to be the result of the horizontal wind exhibiting the same modulation in the vertical as the vertical wind. Lin and Li (1988) reported model results that explained the typical V-shaped cloud top structure of thunderstorms in terms of gravity wave phenomena. However, their choice of motion of the diabatic heating makes their conclusion difficult to interpret in terms of known atmospheric conditions. Robichaud and Lin (1989) summarized the results of many of these simple models of diabatically forced mesoscale circulations. In addition to the study of diabatically forced circulation a similar solution has been

used by many authors over the years to discussed the effects of mountain waves (e.g. Scorer 1949, Crapper 1959, Smith 1980, Durran and Klemp 1983).

Atmospheric interactions are very complex and contributions from a variety of sources combine to give the complete solution. In this thesis we will examine only the contribution of the horizontal wind, moisture and static stability to the linear buoyancy wave solution of the vertical motion field.

1.3 Organization of Thesis

In chapter 2 we describe a steady-state linearized model of a diabatically forced flow in a stably stratified atmosphere. The basic assumptions are discussed to understand the limitations of the model. A numerical method based on a Fast Fourier Transform and a finite differencing scheme in the vertical is introduced. Details of the mathematical treatment and computer model code are given in the appendixes.

The significance of the various model parameters such as the magnitude of the heating term, ambient wind speed and static stability are discussed in chapter 3. We stress the importance of the Scorer parameter (Scorer 1949) that describes the combined effect of the wind shear and static stability in a linearized flow.

In chapter 4 we report on a series of slab-symmetric sensitivity experiments to isolate the effects of various model parameters on the structure and intensity of the vertical motion field. The parameters for which sensitivity is tested include the static stability, shear of the ambient

wind, the amount of momentum dissipation and the pattern of diabatic heating.

Chapter 5 deals with the effects of the ambient wind including wind profiles with a constant first derivative and a constant second derivative, as well as low level jets. These slab-symmetric simulations were performed with model parameters chosen to represent realistic conditions under which local storms are possible. For example, the temperature stratification incorporates the modifying effects of saturated conditions in the diabatic heating layer and also a temperature inversion above the tropopause.

Three dimensional structures of diabatically forced circulations are examined in chapter 6. The effects of the uni-directional wind shear on a "bubble like" heating structure are presented. Furthermore, the sensitivity of the circulation on various amounts of wind blowing perpendicular to the principal wind shear direction is examined.

Chapter 7 applies the three dimensional model to a case study in central Alberta (July 3, 1991). By comparing model results based on the morning and evening soundings, we estimate the buoyancy wave contribution to the vertical motion field. The final chapter discusses the conclusions and areas of further research.

2 Model Formulation and Numerical Method

2.1 Basic assumptions

Our numerical model of the diabatically forced circulation is based on the following assumptions:

1. The atmosphere is stably stratified and the flow is forced by buoyancy due to diabatic heat release.

2. The Boussinesq approximation is valid (i.e. density fluctuations are ignored except in the gravitational terms in the vertical equation of motion).

3. The flow is steady-state. This is essentially the case where the local rate of changes of mean momentum and heat are small compared with their advective changes.

4. The flow is non-rotating (i.e. the coriolis effect can be neglected). Essentially this is valid when the horizontal scale of the circulation is about 100 km or less.

5. The basic state wind and density is the horizontally averaged value over the domain. The perturbation wind and density compared to their basic state values are assumed small such that the products of the perturbation terms can be neglected in the equations of motion (i.e. the linearized equations give the essential dynamics).

6. Turbulent dissipation of momentum is assumed to be small compared to the advective changes and can be approximated with a linear Rayleigh friction formulation. Likewise, divergence of turbulent heat flux is modelled using Newtonian cooling with the Prandtl number set to unity (i.e. the coefficient of Rayleigh heating and Newtonian cooling are equivalent in magnitude).

These assumption are of course not independent of each

other. Essentially, the assumptions are valid for a steady circulation driven by a steady heat source in an environment with significant wind such that the nonlinear effects can be neglected. When applying the model to the atmosphere, we have to keep in mind the limiting factors of the model assumptions.

2.2 Equations of motion

The linear steady-state equations for conservation of horizontal and vertical momentum, conservation of mass and the first law of thermodynamics for a perturbation in an incompressible stratified Boussinesq airflow are given by (e.g. Lin and Li 1988)

$$U\frac{\partial u}{\partial x} + V\frac{\partial u}{\partial y} + w\frac{\partial U}{\partial z} + \frac{1}{\rho}\frac{\partial P}{\partial x} + \beta u = 0 \qquad (2.1)$$

$$U\frac{\partial v}{\partial x} + V\frac{\partial v}{\partial y} + w\frac{\partial V}{\partial z} + \frac{1}{\rho}\frac{\partial P}{\partial y} + \beta v = 0 \qquad (2.2)$$

$$U\frac{\partial w}{\partial x} + V\frac{\partial w}{\partial y} + \frac{1}{\rho}\frac{\partial P}{\partial z} + g\frac{\varrho}{\rho} + \beta w = 0 \qquad (2.3)$$

$$\frac{\partial u}{\partial x} + \frac{\partial v}{\partial y} + \frac{\partial w}{\partial z} = 0 \qquad (2.4)$$

$$U\frac{\partial \varrho}{\partial x} + V\frac{\partial \varrho}{\partial y} - w\rho\frac{N^2}{g} + \beta\rho = -\frac{\rho}{C\overline{T}}q \qquad (2.5)$$

The symbols are as follows: U=U(z) and V=V(z) denote the basic state wind components in the x and y direction, respectively, u, v, w are the time mean perturbation velocities in the x, y, and z direction; P denotes the perturbation pressure; β is the dissipation coefficient; ρ

and ϱ are the basic state density and the perturbation density; g is the acceleration due to gravity; $N^2 = N(z)$ is the Brunt-Väisälä frequency; T is temperature ; C is the heat capacity of air at constant pressure; and q is the heating (or cooling) rate of the diabatic heat source.

The boundary conditions are assumed to be:

1. There is no motion through the bottom and top of the domain (D) (i.e. $w(z=0) = w(z=D) = 0$).

2. There is no transport of heat and momentum through the top and bottom boundaries.

3. Periodic conditions are assumed at the lateral boundaries.

Combining the governing equations and boundary condition (Appendix 1) we have a single equation for the vertical velocity w given by

$$(U\frac{\partial}{\partial x} + V\frac{\partial}{\partial y} + \beta)^2 \nabla^2 w - (U\frac{\partial}{\partial x} + V\frac{\partial}{\partial y} + \beta)$$

$$(\frac{\partial^2 U}{\partial z^2}\frac{\partial w}{\partial x} + \frac{\partial^2 V}{\partial z^2}\frac{\partial w}{\partial y}) + N^2 \nabla_H^2 w = \frac{g}{CT}\nabla_H^2 q \qquad (2.6)$$

where

$$\nabla^2 = \frac{\partial^2}{\partial x^2} + \frac{\partial^2}{\partial y^2} + \frac{\partial^2}{\partial z^2} \qquad \nabla_H^2 = \frac{\partial^2}{\partial x^2} + \frac{\partial^2}{\partial y^2}$$

Note that in (2.5) [and thus in (2.6)] it is assumed that the heat source does not move. For the case of a moving heat source, the basic state wind has to be adjusted by a Galileian transformation (i.e. we obtain the "effective" wind by subtracting the speed of the heat source from the ambient wind). Equation (2.6) is a linear second order partial differential equation with Dirichlet boundary

conditions at z = 0 and z = D. It is the Boussinesq form of the forced Taylor-Goldstein equation which is commonly used in meso-scale dynamics (e.g. Cram et al 1992)

2.3 Numerical method

Equation (2.6) can be transformed into Fourier space using the transformation x-->k and y-->l

$$\frac{\partial^2 \hat{w}}{\partial z^2} + \left[\frac{-\left(k\frac{\partial^2 U}{\partial z^2} + l\frac{\partial^2 V}{\partial z^2}\right)}{R} + \left(\frac{N^2}{R^2} - 1\right)K^2\right]\hat{w} = \frac{gK^2}{CTR^2}\hat{q} \qquad (2.7)$$

where

$$K^2 = k^2 + l^2 \qquad R = kU + lV - i\beta$$

and the double Fourier transform is defined by

$$\hat{w}(k,l,z) = \frac{1}{4\pi^2}\int_{-\infty}^{\infty}\int_{-\infty}^{\infty} w(x,y,z)\, e^{i(kx+ly)}\, dxdy$$

$$\hat{q}(k,l,z) = \frac{1}{4\pi^2}\int_{-\infty}^{\infty}\int_{-\infty}^{\infty} q(x,y,z)\, e^{i(kx+ly)}\, dxdy$$

The heating term q(x,y,z) is represented in finite Fourier space using a Fast Fourier Transformation (FFT). The horizontal wave numbers in the x-direction are found from

$$k_i = \frac{2\pi i}{I\Delta x} \qquad i \le \frac{I}{2}\ ; \qquad k_i = \frac{-2\pi(I+1-i)}{I\Delta x} \qquad i > \frac{I}{2}$$

where i is the index number in x-direction, I is the total index number and Δx is the grid interval. Wave numbers are chosen in this way so that the high wave numbers i greater than I/2, which have non-zero coefficients because of aliasing, are treated as small negative wavenumbers - and the utility of the two sided Fourier transform is retained.

A similar method is used to arrive at the wave numbers for the y direction (Smith 1980).

The horizontal and vertical grid lengths are set to 1562.5 meters and 250 meters respectively. The horizontal domain is then set to 64 X 1562.5 meters (100 km) for both x and y coordinates and vertical domain is set to 54 X 250 meters (13 km).

Noting that $\hat{w} = 0$ at $z = 0$ and $z = D$ we can use a centre-differencing scheme and obtain a tridiagonal matrix to solve equation (2.7) by substitution (details can be found in appendix 2).

2.4 Slab Symmetry

Precipitation is often organized in a linear fashion consisting of bands or arcs (e.g. squall line). The diabatic heating associated with precipitation bands also exhibits a linear pattern, where the heating varies much more in the cross-band direction than in the along-band direction.

Ideally, one should use a three-dimensional circulation model so there is no constraints imposed on the flow by the geometry of the domain. However, because of the computing constraints of three-dimensional modelling, we often consider slab symmetry which drastically reduces the computing requirement. The computing time required to solve this set of equation on a personal computer in two dimensions is less than 1% of the time required to solve the equations in three-dimensions (much of the time in three dimension evolves from manipulation of large external data files). Two-dimensional slab symmetric models simulate conditions in a single vertical plane, assuming that there

is no variation of quantities in the orthogonal direction.

In three dimensions the results are often difficult to interpret because of the complexity of the fully three-dimensional flow, which contains twisting and veering. It is necessary to ensure that the two dimensional case is understood fully before moving on to the more complex three dimensional case. In addition, the computational demands of a three dimensional model makes it unsuitable for numerous experiments.

Consider the case of a diabatic heating source stretched in the y-direction and remaining at constant strength. Provided the ambient wind is strictly uni-directional in the x-direction, the circulation pattern would consist of a circulation that does not vary in the y-direction. For this situation the model equation (2.6) can be reduced to the x-z plane

$$\left(U\frac{\partial}{\partial x}+\beta\right)^2\left(\frac{\partial^2 w}{\partial x^2}+\frac{\partial^2 w}{\partial z^2}\right) - \left(U\frac{\partial}{\partial x}+\beta\right)\left(\frac{\partial^2 U}{\partial z^2}\frac{\partial w}{\partial x}\right)$$

$$+ N^2\frac{\partial^2 w}{\partial x^2} = \frac{g}{CT}\frac{\partial^2 q}{\partial x^2} \qquad (2.8)$$

Some limitations of slab-symmetric models are discussed by Reuter and Yau (1987).

Most of the sensitivity tests reported in this thesis are based on the slab-symmetric assumption, due to limited computing resources. Chapter 6 and 7, however, use the fully three dimensional flow forced by a local "bubble-like" heating source.

3 Interpretation of the Analytical Solution and the Scorer Parameter

3.1 Analytical solution without dissipation

In this chapter we examine an analytical solution for a diabatically forced circulation with a simple heating structure. The reason for investigating this analytical solution is to have an effective "tool" that will help to clarify the interpretations of the findings reported in later chapters of this thesis.

To obtain a simple analytical solution three basic assumptions are made:

1) The basic state wind is unidirectional blowing in the x-direction.

2) Dissipation is neglected (the effects of friction are discussed in section 3.2).

3) The heating (cooling) pattern has a sinusoidal form in the x-direction, is uniform in the y-direction and obtains its peak value at height z = D/2. Specifically we assume

$$q(x,z) = Q \sin(\frac{\pi}{D}z)\cos(\frac{\pi}{L}x) \qquad (3.1)$$

where L is the width and D is the depth of the heating (cooling) pattern. For later use, it is convenient to introduce a wave number K defined by

$$K^2 = \frac{\pi^2}{L^2} + \frac{\pi^2}{D^2} \qquad (3.2)$$

The specific structure of the diabatic forcing term (3.1) may look stringent, however, this is not the case. Recall that any continuous function can be approximated with a finite Fourier series of the form

$$q(x,z) = \Sigma\Sigma\, Q_{(i,k)} \sin(\frac{\pi}{D} kz) \cos(\frac{\pi}{L} ix) \qquad (3.3)$$

Furthermore, the model equation for the vertical motion field (w) is linear and therefore a solution of (w) is simply the linear superposition of the harmonic terms

$$w(x,z) = \Sigma\Sigma\, W_{(i,k)} \sin(\frac{\pi}{D} kz) \cos(\frac{\pi}{L} ix) \qquad (3.4)$$

where $W_{(i,k)}$ is the response to the heating $Q_{(i,k)}$.

Using the three assumptions above, equation (2.6) governing the vertical motion can be simplified to

$$\frac{\partial^2 w}{\partial x^2} + \frac{\partial^2 w}{\partial z^2} + S^2 w = \frac{g}{CTU^2} Q \sin(\frac{\pi}{D} z) \cos(\frac{\pi}{L} x) \qquad (3.5)$$

where S is the Scorer parameter originally introduced by Scorer (1949):

$$S^2 = \frac{N^2}{U^2} - \frac{U_{zz}}{U} \qquad (3.6)$$

Having dimensions of {length^{-1}}, (S) depends on the static stability, the ambient wind speed (U) and the curvature of the basic state wind (U_{zz}). When (U) varies with height, (S) also varies with height even when (N) remains constant. It should be mentioned that (S) enters prominently in studies of mountain waves produced by topographic barriers (e.g.

Scorer 1949; Crapper 1959, Durran and Klemp 1983).

The analytical solution of (3.3) (subject to the boundary conditions w=0 at x= -L/2 x= L/2 and at z=0,D) is given by

$$w = W\sin(\frac{\pi}{D}z)\cos(\frac{\pi}{L}x) \qquad (3.7)$$

where W is the peak updraft speed given by

$$W=\frac{g}{CTU^2}\frac{Q}{S^2-K^2} \qquad (3.8)$$

The understanding of the analytical solution amounts to interpreting (3.8) which relates the peak updraft (W) to the peak heating rate (Q), the wind profile (U,U_{zz}) and the temperature stratification (N) (as combined in the Scorer parameter) and the spatial dimensions of the heating pattern characterized by (K).

Before interpreting (3.8) a few comments are needed. Recall that we have a steady-state circulation driven by diabatic heating. We implicitly assume that the positive heating is correlated with ascending air motion, to be consistent with diabatic heating due to condensation caused by updrafts. This implies that a positive Q value should yield a positive W value. Thus a steady state circulation is only possible, within the assumptions of the analytical solution, if

$$S^2 > K^2$$

This provides an important constraint on the mesoscale circulation. Essentially, the steady-state assumption

requires that there must be a perfect balance between the heating rate (due to the diabatic forcing) and the cooling due to the ascending air and due to differential temperature advection. This idea is best discussed by considered some special cases.

a) Special case where U = 0

For a vanishing ambient wind

$$W = \frac{g}{CT}\frac{Q}{N^2} \qquad (3.9)$$

The steady-state circulation requires that the diabatic heating be balanced by the adiabatic cooling associated with ascending motion. The upward vertical velocity depends numerically on the amount of stratification. A neutral stratification would cause extremely large updraft speeds (W approaches infinity as N approaches zero). A steady circulation cannot occur for a unstable stratification, since N < 0 would result in descending motion which contradicts our assumption of diabatic heating due to ascending saturated air.

b) Special case where N = 0

For neutral stratification,

$$W = -\frac{g}{CT}\frac{Q}{U^2}\left[\frac{U_{zz}}{U} + K^2\right]^{-1} \qquad (3.10)$$

A steady-state circulation can only occur for the case where

$$\frac{U_{zz}}{U} + K^2 < 0$$

For $U_{zz} > 0$ and $U > 0$ a proportion of the diabatic heating is removed by the differential horizontal advection of heat at various levels. For $U_{zz} < 0$, $U_{zz} < -UK^2$ and $U > 0$ the proportion of diabatic heating removed by differential horizontal advection is significantly reduced. It should be noted that $U_{zz} > 0$ implies shear in the upper level is greater than shear in the low levels, whereas, $U_{zz} < 0$ implies low level shear is greater than upper level shear.

The relationship between (W) and (Q) in (3.8) is simple. Provided that all other parameters remain constant, the peak updraft (W) is directly proportional to the peak heating rate (Q). This linear relationship is consistent with the well-known fact that the rate of diabatic heating (i.e. rate of condensation) is proportional to the upward motion of saturated air (e.g. Rogers 1979; pp 41).

The sensitivity of (W) to (U) is best illustrated by taking the partial derivative of equation (3.8) with respect to (U) (while keeping U_{zz}, N, K, and Q constant). This gives

$$\frac{dW}{dU} = \frac{\frac{g}{CT}\frac{Q}{U^4}[2UK^2 + U_{zz}]}{[-K^2 + S^2]^2} \qquad (3.11)$$

As mentioned before, a steady-state circulation requires $S^2 > K^2$. We note that for an ambient wind given by

$$U = -\frac{U_{zz}}{2K^2} \qquad (3.12)$$

the updraft speed has a local minimum given by

$$W = \frac{g}{CT}Q\left[\frac{U_{zz}^2}{4K^2} + N^2\right]^{-1} \qquad (3.13)$$

As the magnitude of (U) increases or decrease from this value (3.12) the magnitude of (W) also increases and approaches infinity as S^2 approaches K^2 or in terms of (U)

$$U \to \pm\sqrt{\frac{N^2}{K^2} + \frac{1}{4}\frac{U_{zz}^2}{K^4}} - \frac{U_{zz}}{2K^2} \qquad (3.14)$$

This implies for a given heating pattern, Brunt-Väisälä frequency and constant shear amount, there exists an ambient wind speed that would result in an extreme value of (W).

Thus, there is a critical combination of parameters that can cause extreme amplification, in agreement with results reported by Robichaud and Lin (1989).

3.2 Analytical solution with dissipation

We will briefly examine the modifying effects of our results if we allow for Rayleigh Friction and Newtonian Cooling. The governing equation of the vertical motion field is

$$(U\frac{\partial}{\partial x}+\beta)^2(\frac{\partial^2 w}{\partial x^2}+\frac{\partial^2 w}{\partial z^2}) - (U\frac{\partial}{\partial x}+\beta)(\frac{\partial^2 U}{\partial z^2}\frac{\partial w}{\partial x})$$

$$+ N^2\frac{\partial^2 w}{\partial x^2} = \frac{g}{CT}\frac{\partial^2 q}{\partial x^2} \qquad (3.15)$$

For the heating pattern (3.1), the solution becomes

$$w = W\sin(\frac{\pi}{D}z)\cos(\frac{\pi}{L}x) \qquad (3.16)$$

where W is the peak updraft speed given by

$$W=\frac{\frac{g}{CT}Q}{U^2[-\frac{\pi^2}{L^2}-\frac{\pi^2}{D^2}-\frac{U_{zz}}{U}+\frac{N^2}{U^2}] - [\beta U(\frac{2\pi}{L}+\frac{2\pi L}{D^2}+\frac{U_{zz}L}{\pi U})\tan(\frac{\pi}{L}x)] + [\beta^2(1+\frac{L^2}{D^2})]}$$

1 **2** **3**

The first term in the denominator is clearly the same as for the case without dissipation. The third term reduces the updraft speed based simply on the amount of dissipation and the aspect ratio of the heating pattern. The second term in the denominator shows that (assuming the heating is a maximum at x=0) near the upwind boundary (-L/2) the vertical velocity will tend to be a weak updraft, whereas, at the downwind boundary (L/2) a weak downdraft exists. The

magnitude of the dissipation decreases to zero at the centre ($x = 0$). Thus at the centre of the grid the vertical velocity is independent of the dissipation term. The combined effect of the dissipation terms is to reduce the intensity of the circulation. The effects of dissipation will be examined in future chapters.

4 Model Parameters and Sensitivity

4.1 Control case

Before investigating the sensitivity of the numerically calculated circulation to various parameters, it is useful to first examine a particular case, referred to as the control case. In this section the values of model inputs will be motivated and the outputs from the model discussed.

Motivation for Choice of Input Parameters

Previous studies (e.g. Lin and Li 1988) assumed that the elevated diabatic heating is stationary and does not move with the ambient flow. Raymond (1986), however, pointed out the importance of including the motion of the diabatic heat source and suggested an indirect method of including this motion into a numerical model. His results show that the diabatic heating term has to move with the wind, unless the heating is from a fixed surface source. Since, diabatic heating is released during cloud formation, the motion of the heat source should closely follow the motion of convective clouds.

Prediction of cloud motion is not without problems. For example, Bluestein and Jain (1985) found that the cloud motion vector usually has a direction similar to the ambient wind at 6 km, whereas, its speed usually is close to that of the wind observed at about 3 km. A reasonable choice, which we have adopted for the control case, is that the diabatic heat source moves with the ambient wind at the base of the

heating layer. Thus the effective basic state wind U_e is given by

$$U_e = U - U_q$$

where U_q is the speed of the heat source. This approach is consistent with the notion that the vertical velocity field is independent of the horizontal wind speed for a flow without shear.

Note: Setting the effective basic state wind to zero at the base of the heat source has implications on interpreting the finding of Lin and Li (1988) and Lin and Chun (1991).

The basic state horizontal wind for the control case (Fig 4.1.1) has a constant shear of 2.5 m $s^{-1}km^{-1}$ and a surface wind speed of 2.4 m s^{-1}.

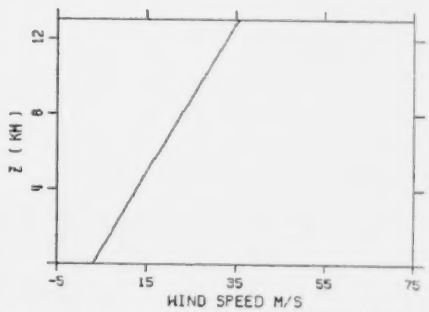

Fig 4.1.1 Control case basic state wind

In this study the heating comes from a slab symmetric source at an elevated height to represent the heating associated with condensation in a convective storm. Assuming that the horizontal and vertical structure are independent of each other the diabatic heating rate can be written as

$$q = Q_0 F(z) G(x)$$

where Q_0 is the maximum heating rate and F and G give the vertical and horizontal structures.

For the control case the horizontal structure is

$$G(x) = \frac{B^2}{(x-\frac{L}{2})^2+B^2} \sin(\frac{5\pi x}{L})$$

Essentially, this structure is a bell shaped curve with half width B which is similar to the structure assumed by Lin and Li (1988) and Robichaud and Lin (1991). However, a sinusoidal wave pattern modifies the bell shaped curve, mainly by changing the sign of the heating term. This formulation allows for diabatic cooling typically found at cloud edges due to evaporation of cloud droplets.

The diabatic heating rate associated with a convective cloud typically becomes a maximum half way through the depth of the heated layer (e.g. Yanai et al 1973). To approximate this vertical structure we assume

$$F(z) = .10\cos[(0.5+\frac{z}{h})\pi] \qquad 0 \le z < h$$

$$F(z) = \cos[(1.5+\frac{z-h}{H-h})\pi] \qquad h \le z < H$$

$$F(z) = .05\cos[(2.5+\frac{z-H}{T-H})\pi] \qquad H \le z < T$$

$$F(z) = 0.0 \qquad T \le z < D$$

where h is the base of the heating source, H is the top of the heating source, T is the tropopause height and D is the depth of the model atmosphere. Note that there is cooling beneath the cloud base that corresponds to evaporation of rain falling from cloud base.

For the control case we will set the half width of the heating term B = 5 km, the base of the heating rate at h =

2 km, the top of the heating rate at H = 8 km and the tropopause at T = 12 km. The structure of the heating rate for the control case with Q_0 = 0.15 J kg^{-1} s^{-1} is shown in Fig 4.1.2. It can be shown that a heating rate of 0.15 J kg^{-1} s^{-1} corresponds to a precipitation rate of approximately 1.0 mm/hr (Holton 1979; p. 327 for details).

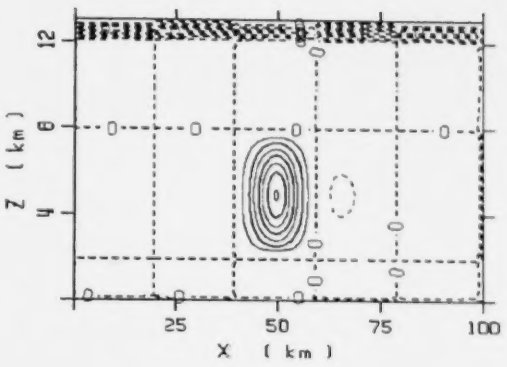

Figure 4.1.2 Heating rate for the control case. Contour interval .02 J $kg^{-1}s^{-1}$ with maximum set to .15 J $kg^{-1}s^{-1}$.

For the control case the vertical structure of the dissipation coefficient (β) is assumed to be

$$\beta(z) = \beta_0 [1 + (4 * \sin(\frac{1000 - z}{1500}\pi))]^2 \qquad 0 \le z < 1 km$$

$$\beta(z) = \beta_0 \qquad 1 \le z < 11 km$$

$$\beta(z) = \beta_0 [1 + 4 * (\sin(\frac{\pi}{2} \times \frac{z - 11000}{D - 11000}))]^2 \qquad 11 km \le z \le D$$

which is similar to that used by Lin and Li (1988). This formulation allows for enhanced dissipation in the lower boundary layer and at the top of the model atmosphere. For the control case the amplitude of the coefficient of Rayleigh heating and Newtonian cooling (β_0) is chosen to be 10^{-4} s^{-1} following Lin and Li (1988).

A typical lapse rate of potential temperature is 3.7 K km^{-1} (Fig 4.1.3). This corresponds to a value of N = 0.011

s^{-1}, which will be used in our control case. Lin and Li (1988) and Robichaud and Lin (1991) used a constant Brunt-Väisälä frequency of N = .01 s^{-1} to model the static stability of the atmosphere.

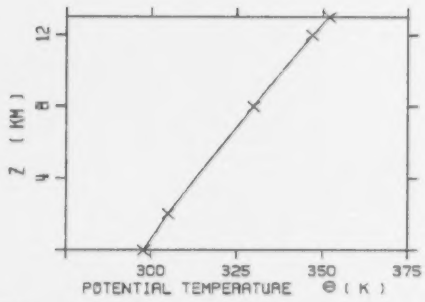

Fig 4.1.3 Control case potential temperature profile.

Results of Control Case

The vertical motion field for the control case is shown in Fig 4.1.4. The updraft is a maximum near the heating centre (x = 50 km and z = 5km). The tilt of the updraft core leans toward the upwind side; this is in agreement with Emmanuel's (1986) findings. Downdrafts are found to the sides of the updraft core with the downwind branch being stronger, which is consistent with downdraft observations in convective storms. The peak downdraft speed of (4.4 cm s^{-1}) is almost 80% of the peak updraft speed (5.2 cm s^{-1}) (refer to table 4.1). The main circulation due to the heating is extended into the upper third of the atmosphere by a downdraft above the core updraft. This upper level feature is forced primarily by conservation of mass and momentum of the air disturbed by the diabatically forced circulation beneath.

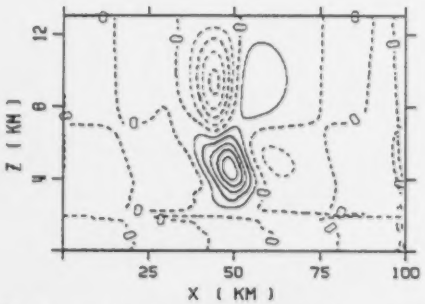

Fig 4.1.4 Control case vertical motion field. Contour interval 1 cm s^{-1}.Solid lines updrafts and dashed lines downdrafts.

4.2 Model sensitivity

The purpose of this section is to gain an understanding of the structure and the strength of the vertical motion field and how sensitive it is to various parameters. Table 4.1 on the next page summarizes the model inputs and output for the sensitivity tests to follow. Case 1 is the control case.

The average kinetic energy of the vertical motion field is defined by

$$KE_w = \frac{\rho}{2M}\sum\sum w^2$$

where M denotes the total number of grid points. This gives a single parameter that quantifies the gross intensity of the circulation.

Model sensitivity to characteristics of the heating source

The sensitivity to the heating is shown in Fig 4.2.1. The amount of heating does not affect the structure of the circulation, but does affect the strength of the perturbed flow. Doubling the heating rate results in doubling the speed of the vertical motion. This proportionality of updraft and heating rate is consistent with our findings based on the analytical solution in chapter 3.

Changing the depth of the heating, has little impact on the peak updraft speed and the average kinetic energy associated (Table 4.1; cases 1, 4, 5, 6), but it does effect the downdraft speed. For example, an increase of depth of

	Input						Output			
Case	N	β	Q_o	H-h	U_q	U_z	Ref Fig	KE_w	W_{max}	W_{min}
1	.011	10	.15	6000	7.4	2.5	1.1	41	5.8	-4.3
2	.011	10	.075	6000	7.4	2.5	2.1b	10	2.9	-2.1
3	.011	10	.30	6000	7.4	2.5	2.1d	165	11.6	-8.6
4	.011	10	.15	5000	7.4	2.5	2.2b	38	5.4	-4.5
5	.011	10	.15	7000	7.4	2.5	2.2d	40	5.9	-3.3
6	.011	10	.15	8000	7.4	2.5	2.2f	40	5.6	-2.3
7	.011	10	.15	6000	0.0	2.5	2.3a	109	5.3	-5.8
8	.011	10	.15	6000	3.7	2.5	2.3b	68	6.0	-5.1
9	.011	10	.15	6000	14.8	2.5	2.3c	21	4.4	-1.7
10	.011	100	.15	6000	7.4	2.5	2.4a	19	4.2	-1.6
11	.011	50	.15	6000	7.4	2.5	2.4b	26	4.8	-2.6
12	.011	5	.15	6000	7.4	2.5	2.4c	50	6.1	-5.2
13	.011	1	.15	6000	7.4	2.5	2.4d	94	6.8	-7.8
14	.0094	10	.15	6000	7.4	2.5	2.5a	90	7.7	-5.7
15	.0124	10	.15	6000	7.4	2.5	2.5b	20	4.4	-2.8
16	.011	10	.15	6000	5.9	1.5	2.6b	21	4.9	-1.8
17	.011	10	.15	6000	9.2	3.5	2.6d	53	4.4	-3.7

Table 4.1 Summary of sensitivity tests. Units of variables presented are N= s^{-1}, β= 10^{-5} s^{-1}, Q_0= J kg^{-1} s^{-1}, H-h= m, U_q= m s^{-1}, U_z= m $s^{-1}km^{-1}$, KE_w=J km^{-3}, W_{max}= cm s^{-1}; W_{min}= cm s^{-1}. Control case is case 1.

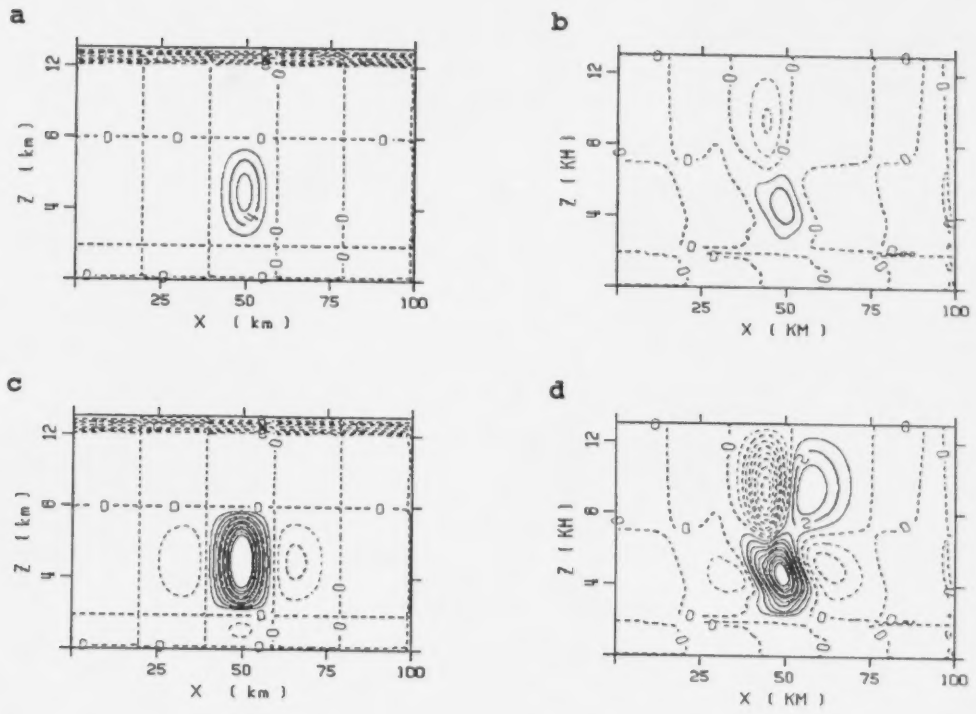

Figure 4.2.1 Magnitude of the diabatic heating rate and corresponding vertical motion fields. Maximum diabatic heating in (a) (case 2) is .075 J $kg^{-1}s^{-1}$ and .30 J $kg^{-1}s^{-1}$ for (c) (case 3). Contour interval for heating rate 0.2 J $kg^{-1}s^{-1}$ to a maximum of .15 J kg^{-1}s-1. Contour interval for vertical velocity 1 cm s^{-1} to a maximum of 10 cm s^{-1}.

the heating layer by 1 km results in a decrease of the peak downdraft of 20-25% while little change in the updraft is noted. However, the downwind tilt of the updrafts above 8 km becomes substantially less as the depth of the heating is increased (fig 4.2.2). This is likely forced by conservation of mass and momentum of the air disturbed directly below by the diabatic heating.

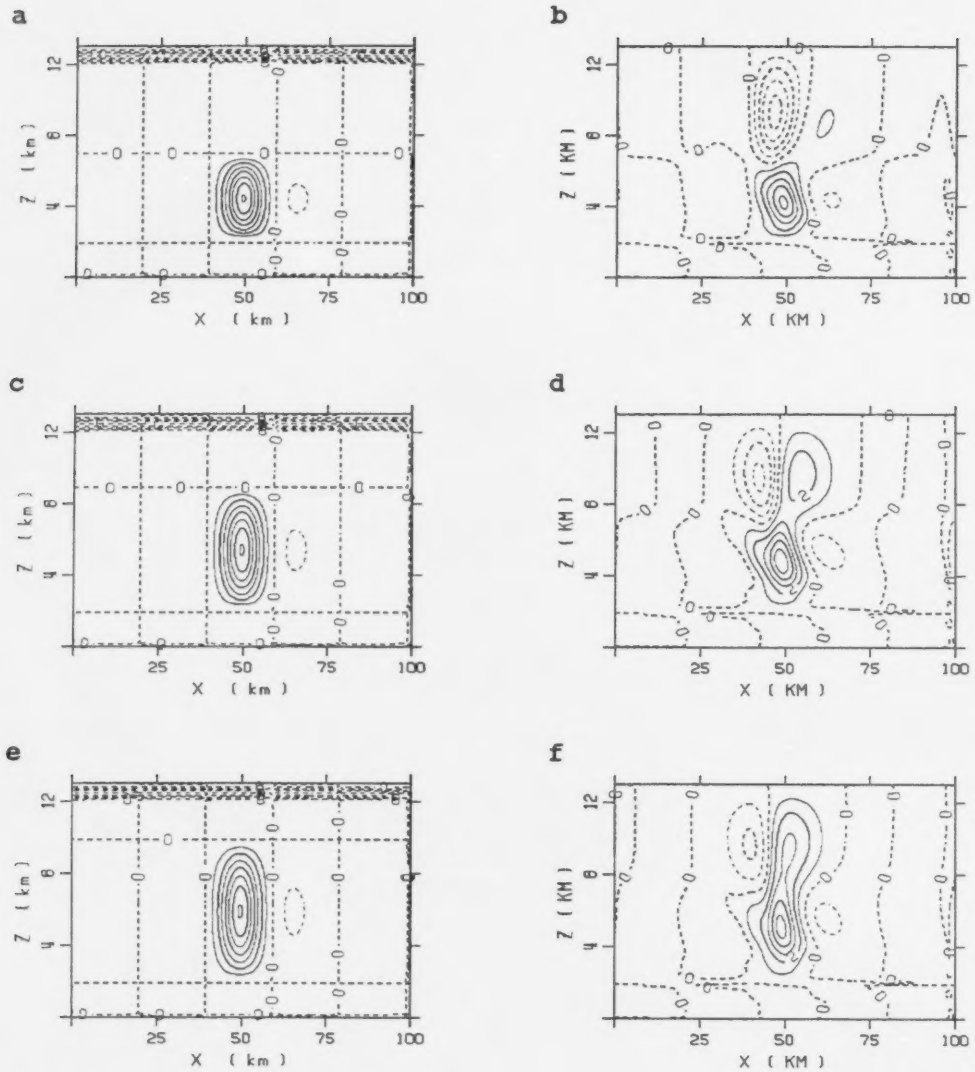

Figure 4.2.2 Depth of the diabatic heating rate and corresponding vertical motion fields. Contour interval for heating rate 0.2 J $kg^{-1}s^{-1}$ to a maximum of .15 J kg^{-1}s-1. Contour interval for vertical velocity 1 cm s^{-1} to a maximum of 10 cm s^{-1}. In table 4.1 (b) is case 4, (d) is case 5 and (f) is case 6.

Sensitivity tests (not shown) revealed that expanding the width of the heating source does not change significantly the peak magnitudes of updrafts and downdrafts, however, it widens the horizontal area associated with upward motion. In addition, we investigated the sensitivity of the circulation on the amount of diabatic cooling surrounding the heating source. While the downdrafts became stronger with an increase in cooling, the updraft core remained unaffected.

Model sensitivity to the speed of the diabatic heat source

We now report on the sensitivity of the vertical motion field to the speed of the diabatic heat source. The upper-level air motion (above 8 km) is substantially changed as the speed of the heat source varies (Fig 4.2.3, Table 4.1). For example, with a stationary heat source the vertical motion field becomes very strong. Clearly, the motion of the diabatic heating rate is an important parameter to take into account when comparing model results to observed atmospheric conditions.

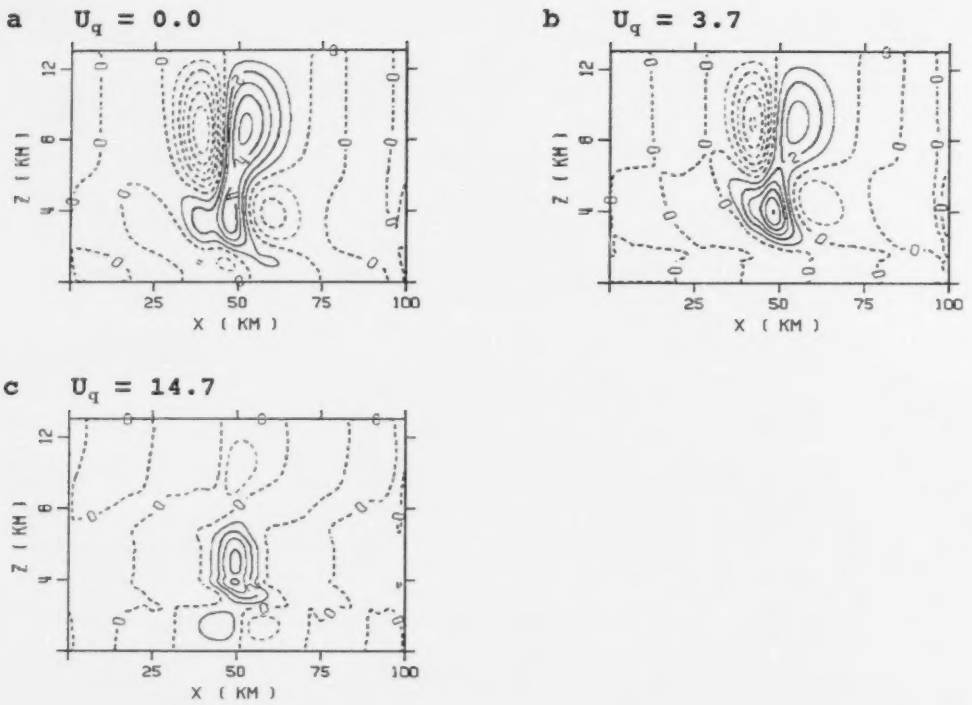

Fig 4.2.3 Vertical velocity field as the speed of the heat source is changed from 0 m s^{-1} in (a) (case 7) to 3.7 m s^{-1} in (b) (case 8) to 14.7 m s^{-1} in (c) (case 9).

Model sensitivity to the dissipation coefficient

The effects of the dissipation coefficient are examined by changing the value of β, while keeping the other parameters constant.

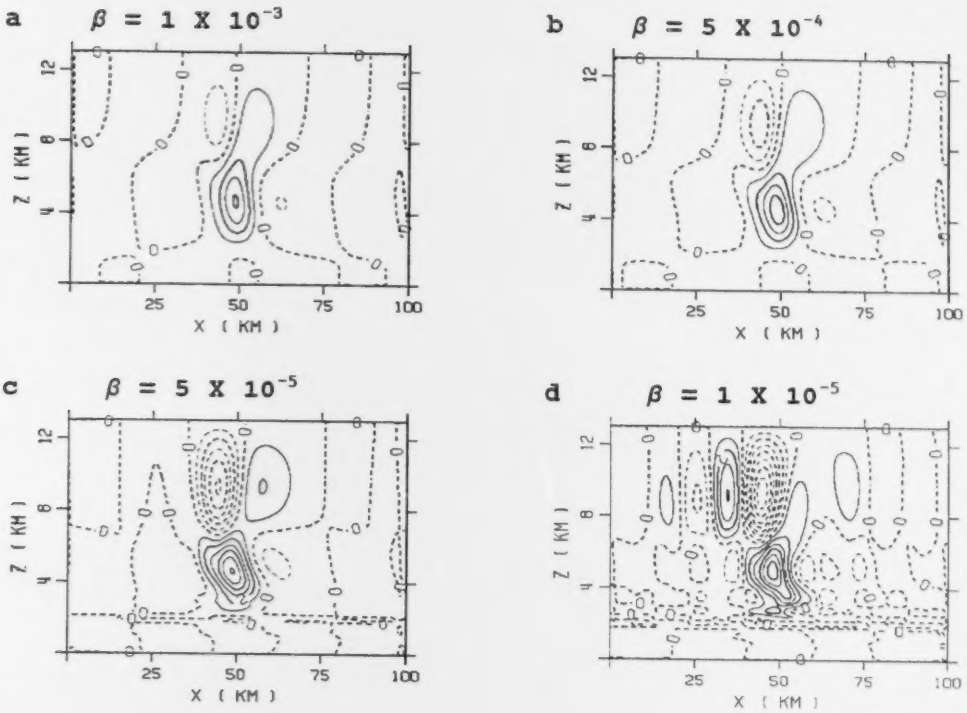

Fig 4.2.4 Comparison of vertical velocity field using different values for the coefficient of Rayleigh friction and Newtonian cooling. For reference to table 4.1 (a) is case 10, (b) is case 11, (c) is case 12 and (d) is case 13.

Table 4.1 (cases 1, 10, 11, 12 and 13)show that a decrease in the dissipation coefficient causes an increase of the updraft speed. In addition, the vertical motion field is enhanced significantly above 8 km and the upwind tilt below 8 km becomes more pronounced (Fig 4.2.4). This indicates that part of the mechanism involved in producing the upwind tilt is associated with this friction. Increasing the dissipation parameter β causes increased smoothing of the vertical motion field. Increasing $\beta = 10^{-5}$ s^{-1} to $\beta = 10^{-3}$

s^{-1} decreases the value of the peak updraft by close to 40%.

Model sensitivity to the Brunt-Väisälä frequency

The degree of static stability of the atmosphere is given in this model by the Brunt-Väisälä frequency (N). Fig 4.2.5 shows the vertical motion fields for N = .0094 s^{-1} and N = .0124 s^{-1} corresponding to potential temperature lapse rates of 2.7 K km^{-1} and 4.7 K km^{-1} respectively. This compares, for the control case of N = .011 s^{-1}, to a lapse rate of 3.7 K km^{-1}.

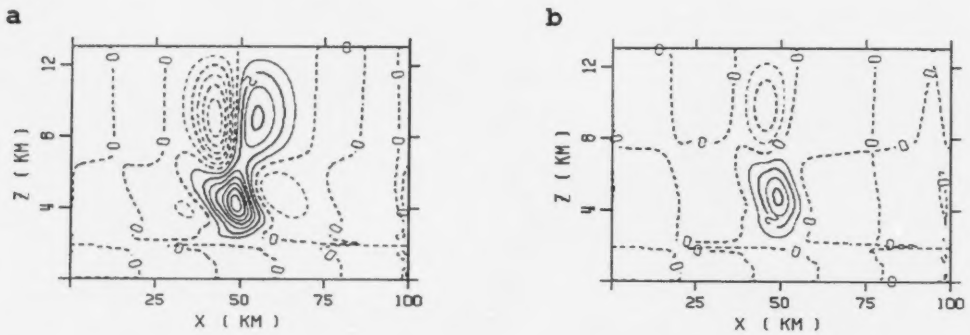

Figure 4.2.5 Vertical motion fields for N = .0094 s^{-1} (a or case 14) and N = .0124 s^{-1} (b or case 15). Contour interval for vertical velocity 1 cm s^{-1}.

For weak static stability, the vertical velocity field is strong, whereas, for strong static stability the vertical velocity field is weak. The upwind tilt of the vertical velocity field is also enhanced for strong static stability. Cases 14 and 15 show a pronounced effect of static stability on the vertical motion field. An increase of static stability of approximately 25% gives a decrease of 89% of

the KE_w and approximately 50% decrease in the peak drafts.

In the atmosphere the stability can vary quite substantially from one layer to the next. In order to compare atmospheric results to model results it will be necessary to ensure that a realistic vertical variation in static stability is included in the model.

Model sensitivity to the vertical shear of the horizontal wind

We now examine the effects of the magnitude of the vertical shear on the horizontal wind. Fig 4.2.6 compares a low shear case (1.5 m s^{-1} km^{-1}) with a high shear case (3.5 m s^{-1} km^{-1}). The enhanced shear produces a very deep upright circulation extending up to 12 km.

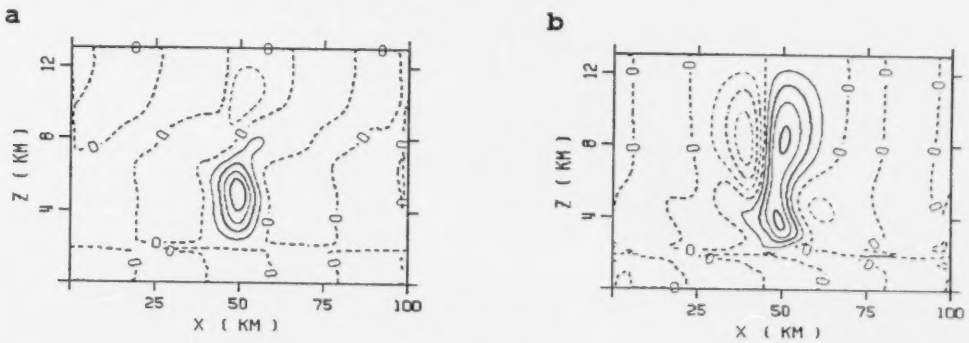

Figure 4.2.6 Vertical motion fields associated with a constant shear of 1.5 m s^{-1} km^{-1} (a or case 16) and a constant shear of 3.5 m s^{-1} km^{-1} (b or case 17). Contour interval for vertical velocity 1 cm s^{-1} to a maximum of 10 cm s^{-1}.

Although the differences in the vertical motion field presented in Fig 4.2.6 are obvious, the relationship between

the wind shear U_z and the maximum and minimum vertical velocity is not. An increase in shear from 1.5 to 2.5 m s^{-1} km^{-1} (control case) results in the peak updraft increasing by 16%, the peak downdraft increasing by 59% and the kinetic energy increasing by 50% (Table 4.1). Whereas, when the wind shear increases from 2.5 to 3.5 m s^{-1} km^{-1} the peak updraft decreases by 24% and the peak downdraft decreases by 14% but the kinetic energy increases by 30%. This implies that the vertical velocity does not necessarily increase as the magnitude of the wind shear increases.

We should point out that the numerical results, for the high wind shear case (case 17), may have been affected by reflection at the top boundary of the domain which forces a w = 0. For a deeper domain the updraft strength may have been more intense at upper levels. Of course, in nature the atmospheric stratification exhibits a tropopause with a temperature inversion which tends to put a "lid" on the circulation. In the next chapter, we will include a more realistic profile of static stability that will result in a natural dampening of the vertical motion in the stratosphere. The effect of changing the wind shear will be examined carefully for the more realistic stratification.

4.3 Discussion

So far we have changed only one model parameter while keeping the others constant. Of course, in nature several parameters can change simultaneously and it is interesting to estimate the combined effect of the variation of several model parameters.

It is known that in atmospheric dynamics the total effect of changing a few atmospheric conditions can exceed

the sum of the individual contributions (Uccellini et al 1987). This so-called synergistic enhancement process occurs through non-linear effects of the various processes. Our linear model cannot copy such a synergistic interaction.

However, our results suggest that similar circulations can be obtained by changing either the Brunt-Väisälä frequency (N), the vertical shear or a linear combination of the two (Fig 4.2.5 and Fig 4.2.6). Likewise, a decrease in N has a similar effect on the vertical motion field as an increase in the depth of the heating rate (Fig 4.2.2 and Fig 4.2.5).

Combining the results of the sensitivity experiments we find that very intense updraft speeds will arise if we have the following conditions; moderate wind shear, very weak static stability, very small dissipation coefficient and a deep intense heat source. This "optimal" combination of parameters is consistent with our parameter analysis discussed in chapter 3 and also with the finding of previous studies (e.g. Weisman and Klemp 1982; Wilhelmson and Klemp 1981; Takeda 1971)

5 Changes in the Vertical Motion Fields due to Wind Shear

In this chapter we investigate how the vertical motion field responds to various profiles of the ambient wind for a stably stratified flow with embedded diabatic heating associated with cloud condensation.

5.1 Vertical stratification of static stability

Throughout this chapter, we assume that the basic state thermal stratification is specified by the potential temperature profile depicted in Fig 5.1.1. The sounding exhibits four separate layers:

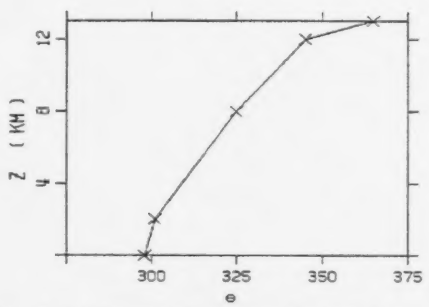

Fig 5.1.1 Potential temperature profile

(i) A "subcloud" layer: from 0-2 km - weakly stable (1.5 K km^{-1}).

(ii) A "cloudy" layer: from 2-8 km - moderately stable layer which will include the diabatic heating associated with convective clouds (4.5 K km^{-1})

(iii) A upper tropospheric layer: from 8-12 km - moderately stable layer (3.5 K km^{-1})

(iv) A stratospheric layer: from 12-13 km - very stable (15 K km^{-1})

In the layer (i), (iii), and (iv) the associated Brunt-Väisälä frequency is computed using

$$N_d^2 = \frac{g}{\theta}\frac{d\theta}{dz}$$

resulting in N = 0.007 s^{-1}; 0.010 s^{-1} and 0.022 s^{-1} respectively. However, in the cloudy layer (2-8 km) the so-call saturated (or moist) Brunt-Väisälä frequency N_m is used. The release of latent heat by condensation partially compensates for the cooling produced by adiabatic expansion, so the density difference between the parcel and the surrounding air is less. Hence, the buoyancy restoring force is decreased. Without allowing for the compensation in the reduced buoyancy restoring-force, the oscillation frequency would be too large. Durran and Klemp (1982) compared expressions used to estimate the moist frequency N_m for various temperature regimes. Based on linear regression of their data, we have estimated N_m as a function of temperature and N_d.

$$N_m^2 = N_d^2 - \left(\left(\frac{(T-238)}{45}\right) x10^{-4}\right) \quad for\ T \geq -35^0 C \quad h \leq z \leq H$$

Note: Due to the model assumption of a stably stratified atmosphere the static stability is assumed to be never less than zero.

5.2 Constant Shear of the ambient wind

To investigate the effects of the amount of shear of the ambient wind on the upward motion, four experiments were made differing only in the amount of constant shear. Fig 5.2.1 shows the chosen wind profiles and the associated vertical motion fields. In all four cases, the surface wind was 2.4 m s^{-1} and the wind speed above z = 12 km is reduced to simulate the condition normally found at the tropopause.

The results indicate that the vertical motion field is very sensitive to the amount of constant shear. For the weak shear case (a), the area of upward motion almost coincides with the area of diabatic heating (see Fig 4.1.2). As the shear is increased, the updraft region becomes progressively deeper and a secondary local maximum of upward motion develops at about z = 9 km on the downwind flank. For the extreme wind shear case, with the wind speed being 55 m s^{-1} near the tropopause, the low-level and upper-level circulation cells merge into a single deep cell which is almost upright.

Table 5.2.1 Comparison of the vertical motion field associated with various constant wind shear profiles.

Units for Inputs and outputs as given in table 4.1.

	Output				**Input**	
Fig 5.2.1	W_{max}	W_{min}	KE_W		U_q	V_z
b	6.5	-1.1	36		4.8	1.0
d	8.0	-4.4	68		7.7	2.7
f	9.7	-6.2	134		9.3	3.5
h	9.7	-7.0	255		10.6	4.4

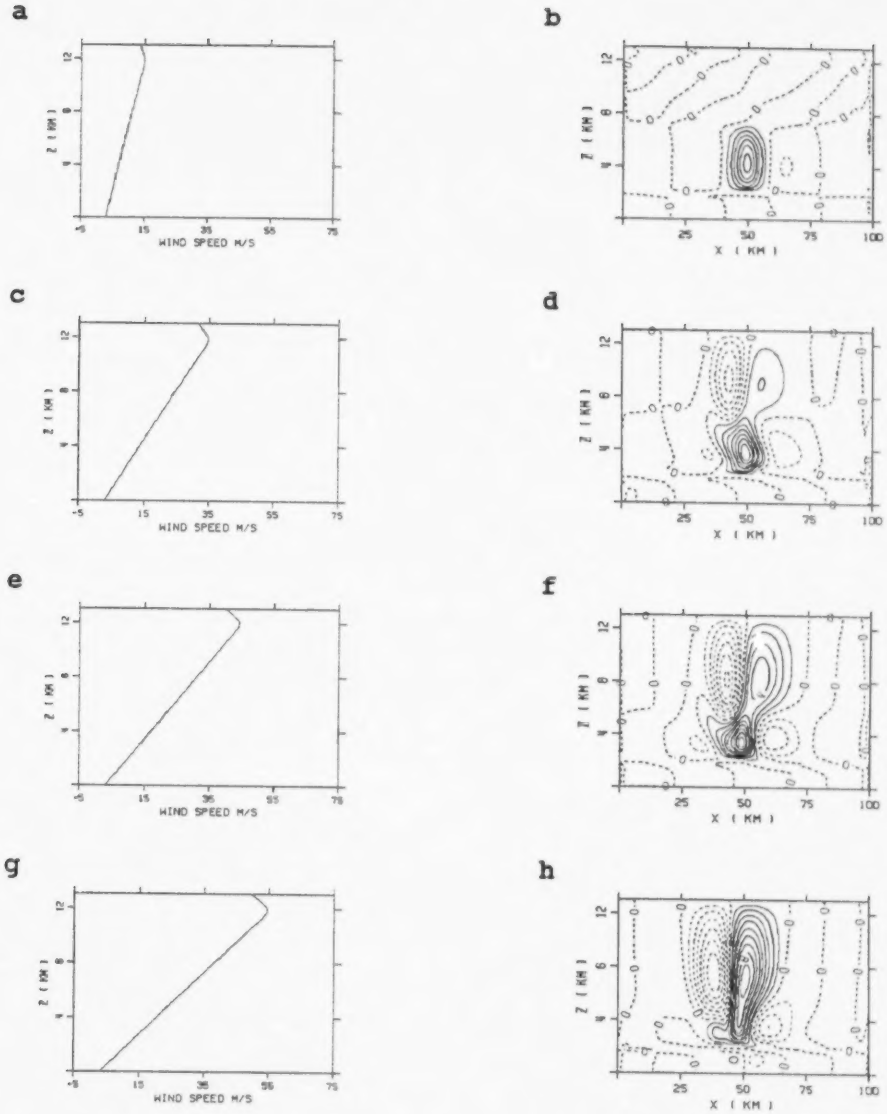

Figure 5.2.1 Wind profiles (constant shear) and corresponding vertical motion fields

The magnitude of the peak updraft and downdraft speed (w_{max} and w_{min}) and the kinetic energy (KE_w) are compared in Table 5.2.1. As the shear increases, the KE_w increases dramatically. Also the peak updraft speed becomes more intense with increasing ambient wind shears, except for the extreme case where the tropopause seems to put a lid on the development of the peak updraft. Peak downdrafts speeds are roughly 2/3 of the upward counterparts. The dominant downdraft occurs on the downwind side of the core updraft, consistent with observations of convective clouds (e.g. Reuter and Yau 1987). The depicted updraft fields show that with increasing shear the location of the maximum updraft speed moves higher up.

5.3 Second derivative of the ambient wind

Having examined the effects of the gross amount of the ambient wind shear, we now shift our attention to the detail of the wind profile. Specifically, we consider a parabolic profile of the ambient wind:

$$U(z) = U(0) + \frac{U(T) - U(0)}{T} z + 4 V_d \left(\frac{1}{T} - \frac{z}{T^2}\right) z$$

where T is the tropopause height and V_d is the deviation from a straight line at height T/2. Fig 5.3.1 shows the results for the four cases V_d =-5, 0, 5, and 10 m s^{-1} with T = 12 km and U(0) = 2.4 m s^{-1} and U(T) = 35 m s^{-1}. The corresponding second derivatives of the wind are .28, 0, -.28 and -.57 m s^{-1} km^{-2}. Clearly, the amount of curvature (i.e. second derivative) in the wind effects the strength of the vertical motion field. The larger the value of V_d, the more intense is the interaction between the upper and lower cells. Table 5.2 compares the w_{max}, w_{min} and the KE_w values of the vertical motion field.

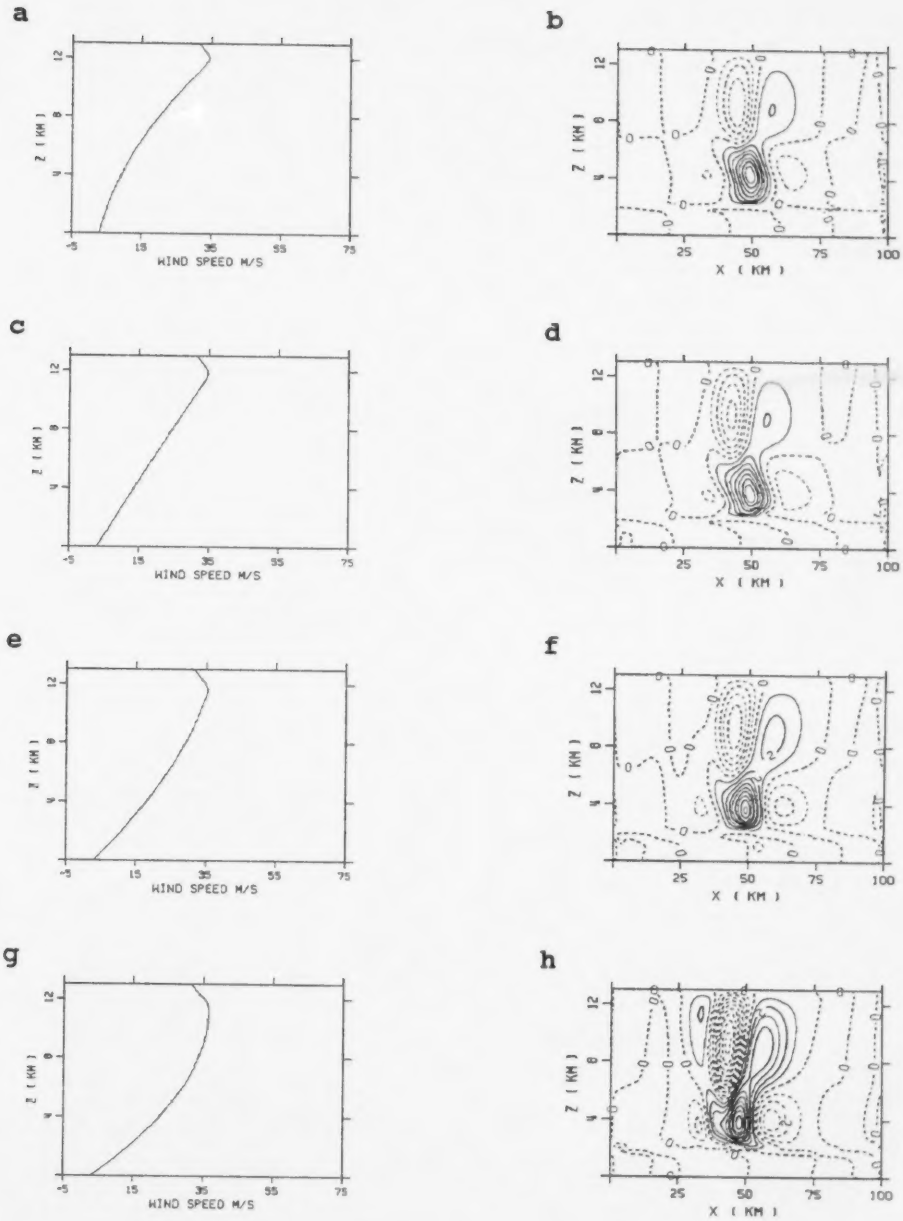

Figure 5.3.1 Wind profiles (non-constant shear) and corresponding vertical motion fields

Table 5.3 Comparison of the vertical motion fields associated with various constant second derivatives of the horizontal wind

Units of inputs and outputs as given in table 4.1. Departure from straight line wind (constant shear) V_d at 6000 m in m s^{-1}

	Output				Input	
Fig 5.3.1	W_{max}	W_{min}	KE_W		U_q	V_d
b	8.0	-4.0	62		5.2	-5.0
d	8.0	-4.4	68		7.7	0.0
f	9.4	-4.9	88		10.1	+5.0
h	10.8	-9.5	204		12.7	+10.0

Doubling the value of V_d from 5 to 10 m s^{-1}, results in an increase of KE_w by 131 %, a consequence of the strengthening of the circulation in upper levels. The peak updraft speed remains the same at 8 cm s^{-1} for both V_d = 0 and -5 m s^{-1}. This result suggests that strong low-level shear is more favourable for updraft enhancement than stronger upper level shear.

Note that for the parabolic wind profile extending from ground to the tropopause, the speed at which the heating source moves varies from U_q = 5.2 m s^{-1} for V_d = -5 m s^{-1} to U_q = 12.1 m s^{-1} for V_d = 10 m s^{-1}. As U_q regulates the effective wind speed (i.e. $U_e = U(z) - U_q$) which determines the horizontal advection, it is difficult to isolate unambiguously the effect of the second derivative of the ambient wind from the effects of a changed U_q. To clarify this issue, we have made another series of experiments for which the wind profile varies only in the layer where the diabatic heating occurs. The profile exhibits a constant

shear above and below the heating layer and has a parabolic profile from z = 2 km to z = 8 km (Fig 5.3.2). The maximum deviation in speed from the constant shear occurs at z = t km and this deviation in wind speed is indicated with V_d^*.

The vertical motion fields indicate that when the shear increases with height ($d^2U/dz^2 > 0$) the circulation consists mainly of a moderately strong updraft roughly co-located with the heating source and a secondary weak updraft in upper-levels. A similar structure is found for the constant shear case ($d^2U/dz^2 = 0$). On the other hand, when the shear decreases with height ($d^2U/dz^2 < 0$) the two cells unite into a single deep cell. Fig 5.3.2 suggests that the deviation V_d^* = 5 m s^{-1} causes a stronger circulation then for the case where the V_d^* = 10 m s^{-1}. Comparing carefully the profiles with V_d^* = 5 and 10 m s^{-1} reveals a major difference. For V_d^* = 5 m s^{-1}, the ambient wind increases with height throughout the heated layer, whereas, for V_d^* = 10 m s^{-1} the ambient wind first increases but higher up decreases again. After numerous experiments with several different parabolic wind profiles we found consistently that increasing the convex bulge of the wind profile enhances the vertical motion field until the bulge leads to a negative shear ($dU/dz < 0$). In other words the strongest vertical motion field occurs when the upper level winds are sufficiently strong such that the wind speed increases everywhere through the heated layer.

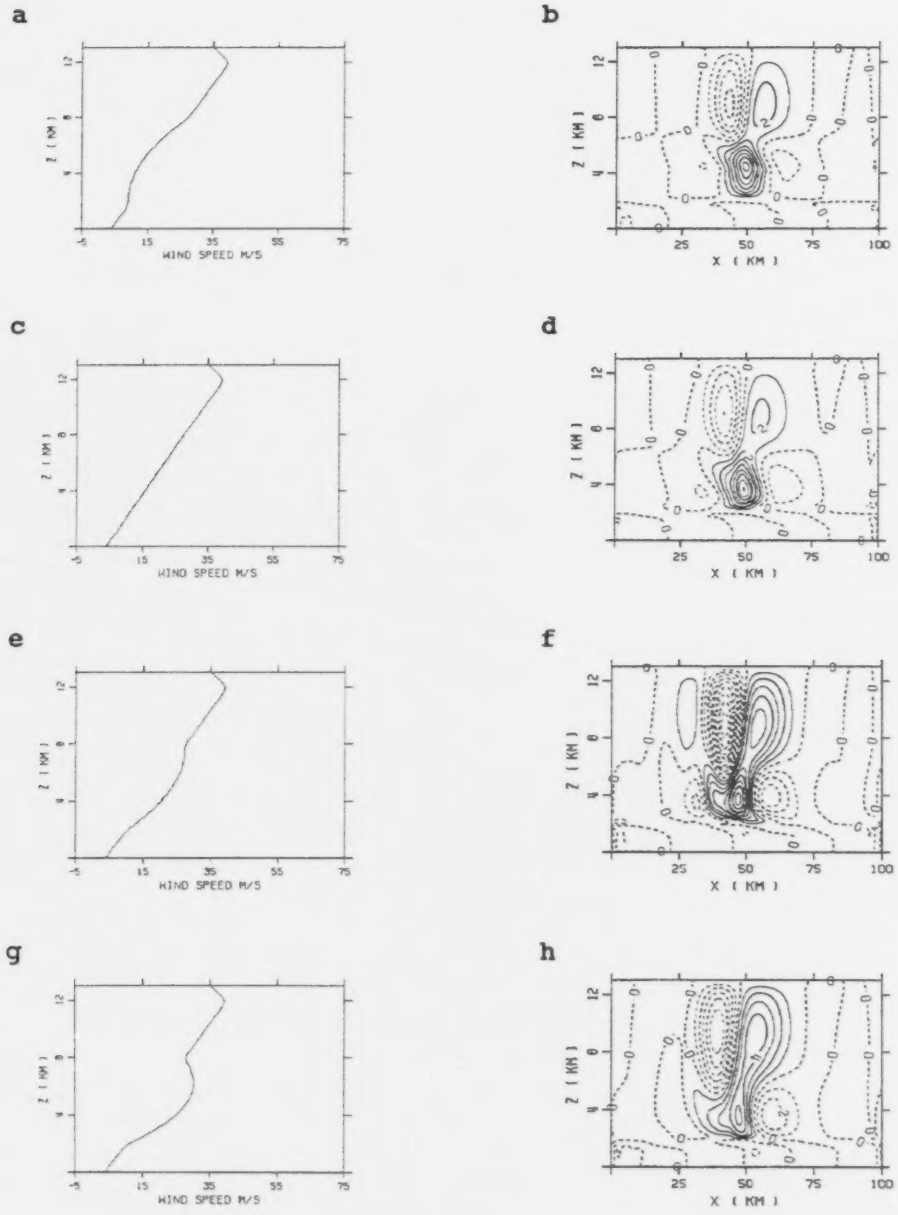

Fig 5.3.2 Wind profiles (non-constant shear in heated layer) and associated vertical motion field

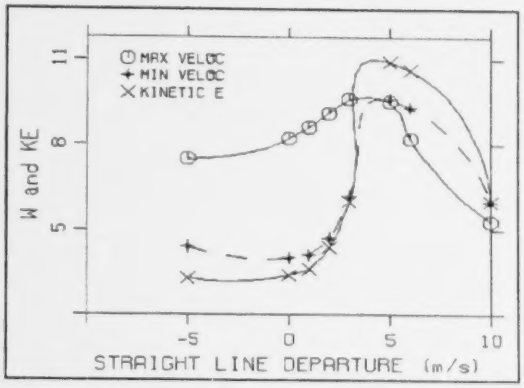

Fig 5.3.3 Intensity of the vertical motion fields associated with various second derivatives of the wind. Maximum and minimum vertical velocities (cm/s). Minimum velocities are negative and maximum velocities are positive. The kinetic energy is in units of 10^{-1} J/km^{-3}. The departure from straight line of the horizontal wind is defined at 5 km.

Fig 5.3.3 shows how the kinetic energy (KE_w) and the maximum and minimum vertical velocities (w_{max} and w_{min}) depend on V_d^*. The peak updraft reaches its maximum at about V_d^* = 3 m s^{-1}, whereas, the peak KE_w peaks at V_d^* = 5 m s^{-1}. The small increase from V_d^* = 3 m s^{-1} to V_d^* = 5 m s^{-1} leads to more than doubling in the value of KE_w. It should be mentioned that numerical modelling studies identified that a wind profile given by a tanh function is very favourable for severe storm development (e.g. Weisman and Klemp 1982), and a tanh function clearly has a positive first derivative (i.e. wind increases with height) and a negative second derivative (i.e. shear decreases with height).

5.4 Low level jet streams

A jet stream is an intense, narrow, quasi-horizontal current of wind that is associated with strong vertical shears. "Intense" usually means at least 30 m s^{-1} for the upper portion of the troposphere and 15 m s^{-1} for the lower portion of the troposphere; whereas "strong" vertical shear is at least 5-10 m s^{-1} km^{-1} (Bluestein 1986).

Low level jets often contribute to the development of Meso-scale Cloud Complexes (MCCs). MCCs are long lived convective weather systems that produce widespread rainfall over continental mid-latitude areas during the spring and summer seasons (Maddox 1980). MCCs usually organize during the evening and reach maximum size around local midnight; about the time that the nocturnal low-level jet stream reaches maximum strength and is located nearest the surface (Hoxit 1975). MCCs tend to weaken during the morning hours when the low level jet is weakening as well.

The presence of a strong low level jet can support a meso-scale updraft in several ways:

i) The vertical shear associated with the jet produces differential advection of heat and moisture to destabilize the lower portion of the troposphere.

ii) The jet is associated with strong low level convergence zones.

iii) The jet often concentrates cyclonic vorticity in low levels.

iv) The jet can support and enhance gravity waves.

In this two dimensional study we are unable to investigate (ii, iii) and so we focus on the gravity-wave enhancement process. Numerical experiments were made with various low-level jet wind profiles while keeping all other model inputs constant. Fig 5.4.1 shows a selection of profiles and associated vertical motion fields. These particular choices of jet profiles are based on the prototypes of Bonner's (1968) classification scheme. The criteria for Bonner's classification scheme is described below.

Bonner's Classification Scheme

Classification 0: Speed of the maximum low level wind be at least 10 m/s.

Classification 1: The wind at the maximum level of the maximum wind must equal or exceed 12 m/s and must decrease by at least 6 m/s to the next higher minimum or to the 3-km level whichever is lower.

Classification 2: The wind at the maximum level of the maximum wind must equal or exceed 16 m/s and must decrease by at least 8 m/s to the next higher minimum or to the 3-km level whichever is lower.

Classification 3: The wind at the maximum level of the maximum wind must equal or exceed 20 m/s and must decrease by at least 10 m/s to the next higher minimum or to the 3-km level whichever is lower.

Table 5.4.1 Comparison of the vertical velocity and kinetic energy associated with low level jets

Units as given in table 4.1.

Classification	0	1	2	3
KE_w	68	80	60	60
W_{max}	8.2	7.8	7.7	7.3

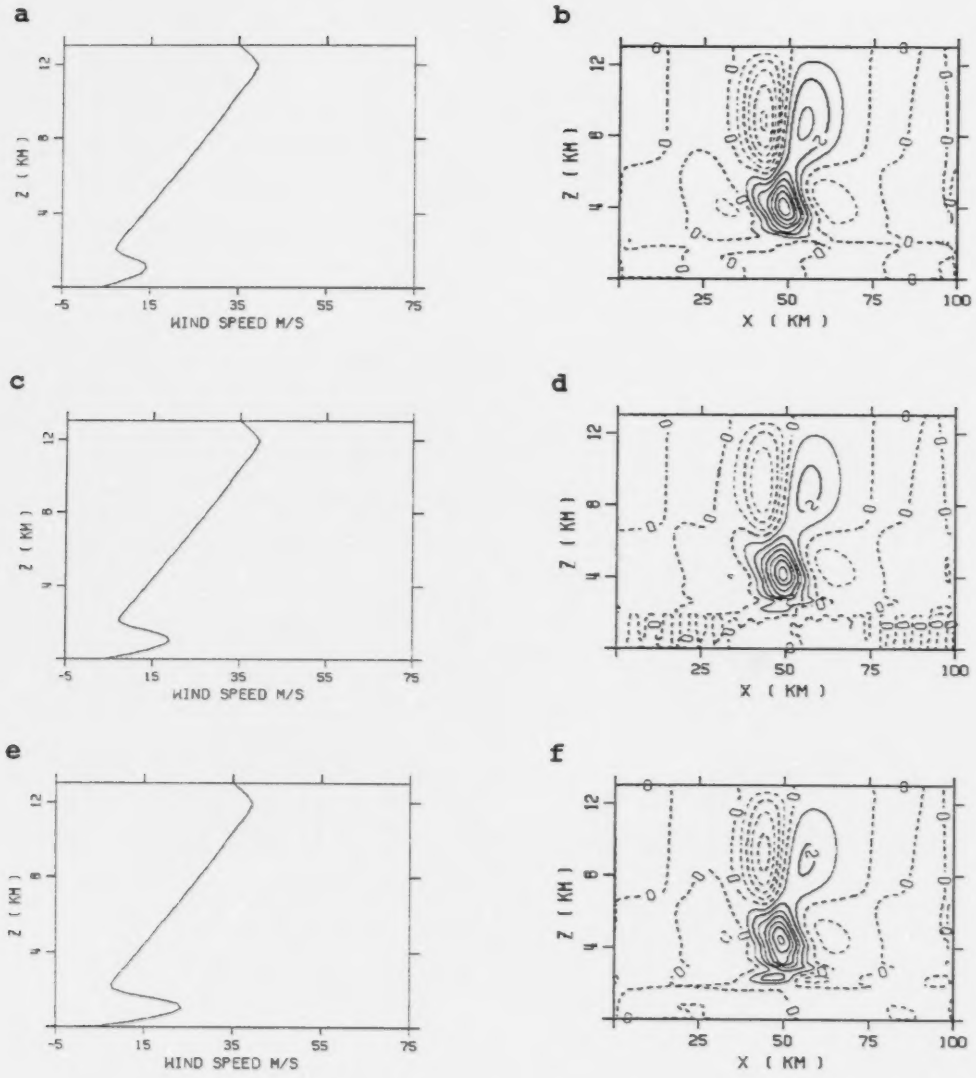

Fig 5.4.1 Low level jets with associated vertical motion fields

The figure shows that the spatial structure of the updraft remains similar even for a very strong low level jet. Furthermore, the peak updraft and the average kinetic energy is relatively insensitive to the particular choice of low level jet profile (Table 5.4.1). These values tend to decrease slightly with increasing jet intensity.

The conclusion to be drawn is that the gravity wave support is <u>not</u> a dominant mechanism to produce a long-lasting upward motion, at least not for the chosen atmospheric stratification.

As mentioned before, the jet stream often provides favourable conditions for differential advection of temperature; warming near the surface and cooling aloft with the net result of reducing the static stability.

Fig 5.4.2 shows the vertical motion field for the case where the Brunt-Väisälä frequency is reduced by 10% corresponding to a 1° C warming near the surface and a 1° C cooling near the cloud top. Clearly, the circulation is much more intense.

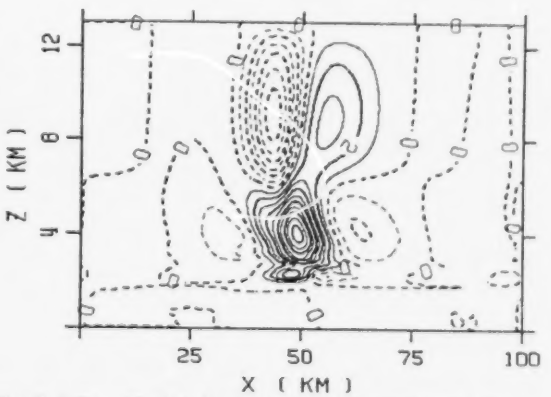

Fig 5.4.2 Vertical motion field associated with a classification 2 low level jet in a destabilized environment

The reduced static stability provides an increase of 120% in the average kinetic energy (Table 5.4.2) and approximately a 40% increase in the peak updraft strength. Obviously, the buoyancy waves are much more sensitive to destabilization of the troposphere (which is a possible

result of the low level jet) than to the presence of the low level jet.

Table 5.4.2 Comparison of the kinetic energy and maximum vertical velocity associated with a classification 2 low level jet with different static stability

Unit as per table 4.1

Classification 2 Jet	Fig 5.4.1d	Fig 5.4.2
KE_W	60	132
W_{max}	7.7	10.7

It is clear that the buoyancy waves are enhanced by the destabilizing of the atmosphere caused by cloud top cooling and warm air associated with the low level jet and only slightly by the presence of the low level jet itself.

If we define the jet in terms of a moving frame of reference some interesting results are achieved.

Table 5.4.3 Kinetic energy and maximum vertical velocity associated with a classification 1 low level jet defined in a moving frame of reference

Classification 1 Jet in moving frame of reference	Fig 5.4.3
KE_W	223
W_{max} cm s^{-1}	11.1

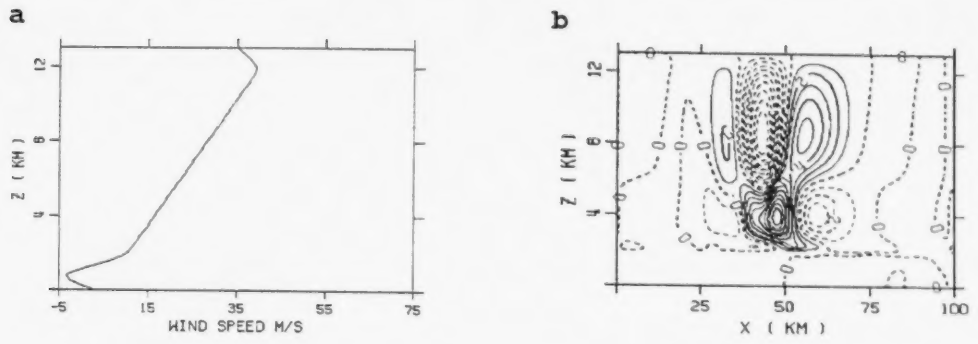

Figure 5.4.3 Wind profile and vertical motion field. Wind profile is a category 1 jet if defined in a moving frame of reference.

It is apparent (Fig 5.4.3 and Table 5.4.3) that the enhancement due to a weak easterly low level jet (category 1 if defined in a moving frame of reference) is greater than the effects of reducing the static stability presented previously (Fig 5.4.2 and Table 5.4.2). We can conclude from this that the vertical motion field is enhanced by buoyancy waves caused by low level jets if we describe the jet within the moving frame of reference used.

5.5 The Scorer Parameter

The effects of the Scorer parameter (S^2) on the vertical velocity field were discussed in chapter 3. It was found that an enhanced vertical velocity field will occur when the magnitude of S^2 is similar to that of the wave number (K^2). To find the magnitude of K^2 the diabatic heating term in the horizontal can be estimated using the function G(x) given in chapter 4.1. The wave number in the vertical is approximated using the heating depth (H-h = 6000 m). Thus

the magnitude of the total wave number K is estimated as

$$K^2 = [\frac{2.5\pi}{32\times250}]^2 + [\frac{\pi}{(6000)}]^2 = 4.7\times10^{-3}m^{-2}$$

Maximum interaction occurs when

$$K^2 = S^2 = \frac{N^2}{U^2} - \frac{U_{zz}}{U}$$

which can be solved for U to obtain

$$U = \sqrt{\frac{N^2}{K^2} + \frac{1}{4}\frac{U_{zz}^2}{K^4}} - \frac{U_{zz}}{2K^2}$$

The resulting profile of U is plotted in Fig 5.5.1.

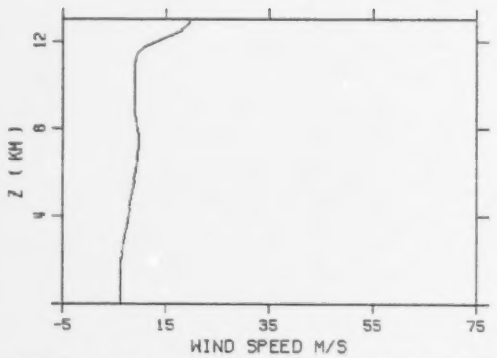

Fig 5.5.1 Wind profile associated with maximum enhancement of the vertical motion field

Fig 5.5.2 depicts the vertical motion field for the case where the heating source is assumed to be stationary (U_q = 0). The strength of the vertical motion field is very strong despite the weak wind shear. However, it is unlikely that the heat source does not move at all and the effective basic state wind would seldom approach this value in nature.

The results indicate how important the Scorer parameter is in enhancing buoyancy waves. Mesoscale circulations with a sheared basic state flow will likely have a layer in which the wave number (K^2) and the Scorer parameter (S^2) are

similar. It is likely that the depth of such a layer determines the intensity of the vertical motion field.

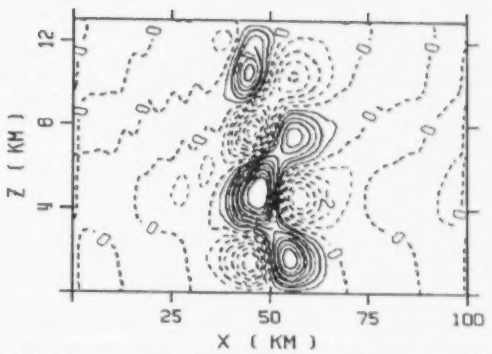

Fig 5.5.2 Vertical motion field using wind profile derived from Scorer parameter to achieve maximum enhancement

To establish an enhanced vertical motion field in a moving frame of reference we will estimate the wind speed in association with the Scorer parameter in the heated layer. This will allow us to estimate the preferred basic state wind for an enhanced vertical motion field in a moving frame of reference (Fig 5.5.3).

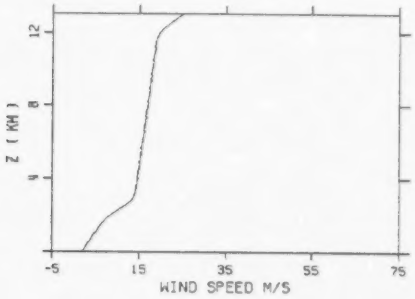

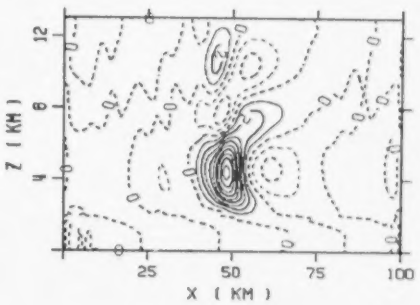

Fig 5.5.3 Estimated effective wind in a moving frame of reference to achieve maximum enhancement of the vertical motion field.

The enhanced vertical velocities (Table 5.5) associated with low wind shears when the magnitude of the horizontal wind is associated with the Scorer parameter is an interesting phenomenum. Even when the speed of the heat source is taken into account one can still find a wind profile with relatively weak wind shear that produces an intense

circulation similar to a strong wind shear case (Table 5.2.1). However, the structure of the vertical motion field is very different (compare Fig 5.5.2 and 5.5.3 to Fig 5.2.1).

Table 5.5 Comparison of vertical velocities and kinetic energy associated with wind profiles calculated to achieve the strongest vertical motion field

Units as per Table 4.1

Figure	W_{max}	W_{min}	KE_w
5.5.2	12.5	-7.4	211
5.5.3	9.3	-2.8	69

The effects of the Scorer parameter and its relationship to the size of a convective cell is interesting. We recommend that an observational study be made to investigate the typical sizes of S^2 and K^2 and whether there exists condition when they have similar magnitudes.

6 Three Dimensional Model Results

In this chapter we present simulation results using the three dimensional (3D) model to investigate three-dimensional aspects of the diabatically forced circulation. In addition, a comparison between the vertical motion fields from the 3D model with those of the 2D model clarifies to what extent our previous finding are valid even when the flow is not restricted to a single vertical plane.

There is a major difference in computing time between the 2D and the 3D model runs. Whereas, the 2D code takes about 10 minutes for execution, the 3D code requires about 16 hours of execution time on our 386 PC. This factor of approximately 100 in additional computing time is mainly due to the need to manipulate large data arrays in external files, since the DOS operating system severely restricts the size of the arrays in the computer core memory.

6.1 3-D model with a slab-symmetric heating structure

First we compare the 3D model results with those of the slab-symmetric model for a case of constant shear blowing in the x-direction. Specifically, we have chosen the diabatic heating structure shown in Fig 4.1.2, the temperature stratification shown in Fig 5.1.1 and the wind profile shown in Fig 5.2.1c. The y-component of the ambient wind profile is set to V = 0, and the heating rate does not vary in y. The results from the two models are very similar. The 3D model gives slightly stronger updrafts above 8 km compared to the 2D case (Fig 6.1.1).

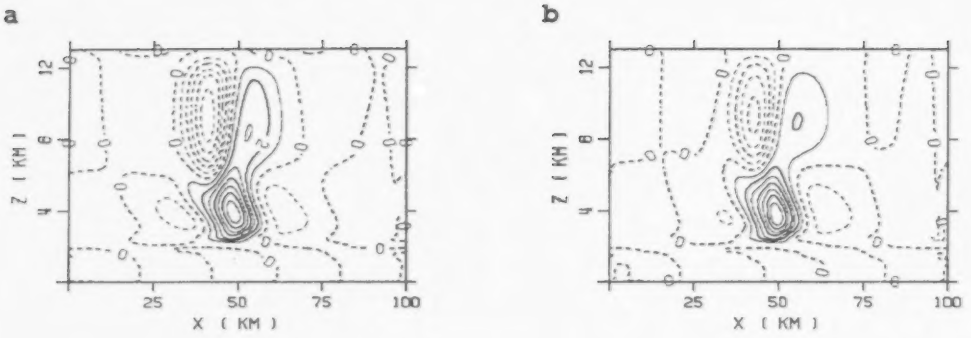

Fig 6.1.1 Comparison of the three dimensional case (a) to the two dimensional case presented in 5.2.1d.

The next 3D experiment was made to simulate the situation where the line heating is oriented parallel to the basic state flow. Essentially all model input parameters remain the same as the previous run except that U = 0 and V is a function of z depicted by the linear wind profile in Fig 5.2.1c.

The results of this experiment (Fig 6.1.2) indicate a disturbance that is located at the heating source region. Clearly, the basic state wind blowing in the y-direction cannot advect any heat, since the thermal gradient in the y-direction is zero. In fact, the specific choice of the V profile is immaterial as it cannot contribute to the

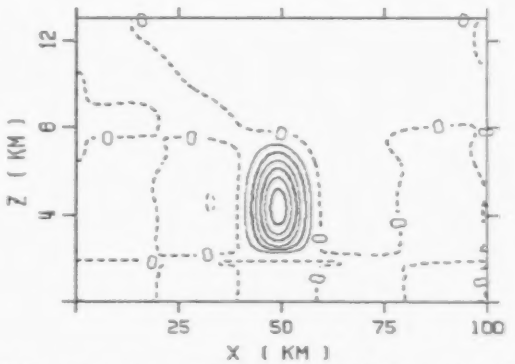

Fig 6.1.2 Vertical motion field associated with the wind parallel to the gradient of heating

updraft enhancement. This has a major implication for our slab-symmetric findings. In those experiments we had assumed that the ambient wind blows exactly perpendicular to the slab of diabatic heating. Now we find that it does not matter what the magnitude of the along-band wind component is as it does not contribute to an enhanced vertical motion field. The bottom line is that only the wind component perpendicular to the heating line is of relevance for a strictly slab-symmetric heating source. If baroclinic effects were to be included in our linearized buoyancy wave model, the amount of the windshear parallel to the heating line would become important as shown by Robichaud and Lin (1991).

6.2 3D model results with a three-dimensional heating source

Up to now we have always assumed that the heating has a slab-symmetric structure that does not vary in the y-direction. Our attention now focuses on a three-dimensional heating source that has a circular shape in the horizontal. This "bubble like" heating source has a heating rate that decreases as the radius increases according to a bell-shaped curve modified with a sinusoidal wave pattern as described in section 4.1. Details of the prescribed heating source can be taken from the model code given in appendix 2. The 3D heating structure forces a fully three-dimensional circulation pattern even for uni-directional wind.

Fig 6.2.1 compares the vertical motion field of the vertical section through the centre of the heating for three values of constant uni-directional shear in the x-direction (1.9, 2.7 and 4.4 m s^{-1} km^{-1}) and V = 0. The chosen wind profiles have been plotted in Fig 5.2.1a, c and g

respectively. The results (Fig 6.2.1) indicate that the increasing wind shear is accompanied with an increasing disturbance in the vertical motion field. In fact, the vertical motion fields are almost identical in structure to those from the slab-symmetric model (see Fig 5.2.1).

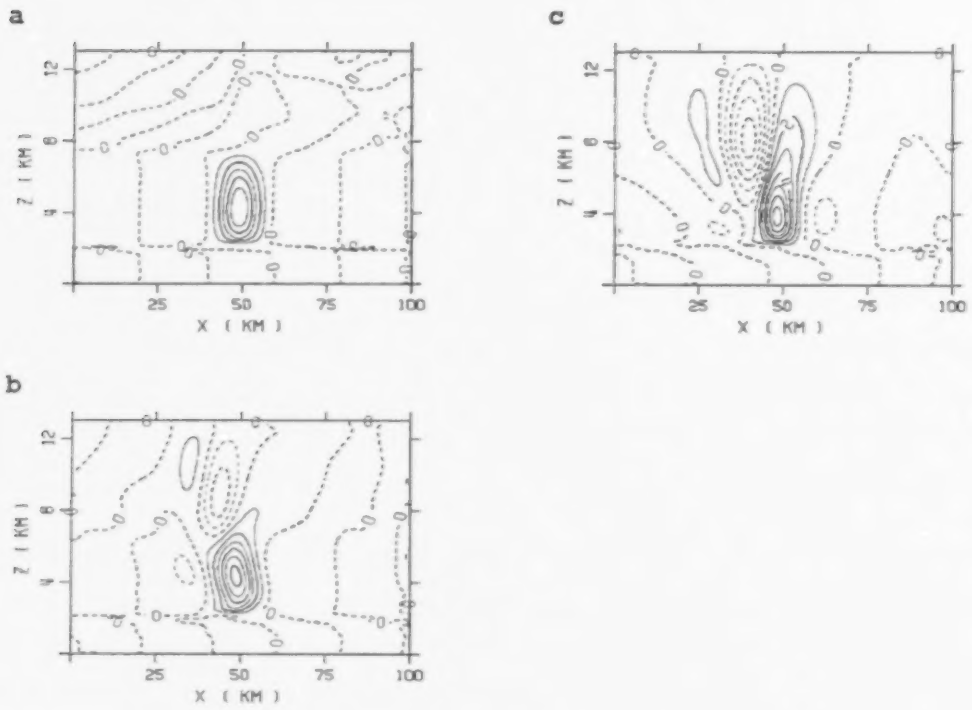

Fig 6.2.1 Three dimensional vertical motion fields for a "bubble like" heating source and constant shear. x-z contour plots at centre of grid (y=50 km). Unidirectional wind; U = 1.0 m $s^{-1}km^{-1}$ (a); U = 2.7 m $s^{-1}km^{-1}$ (b); U = 4.4 m $s^{-1}km^{-1}$ (c)

Table 6.2.1 Comparison of the vertical velocities and the kinetic energy associated with a "bubble like" heating source in with various uni-directional constant shear

Units the same as in table 4.1.

Fig 6.2.1	W_{max}	W_{min}	KE_w
a	6.1	-1.0	2.0
b	6.4	-2.7	3.0
c	7.4	-4.6	6.1

Also the values of W_{max}, W_{min} and KE_w show a similar trend for both 2D (Table 5.2.1) and 3D (Table 6.2.1) model runs. The impact of increasing the ambient shear is more significant (i.e. the magnitude of the vertical velocities) for the slab-symmetric case, since in the "bubble like" heating the ambient flow can pass around the updraft that tends to produce an obstacle to the flow. This finding is consistent with numerical cumulus cloud simulations (e.g. Reuter and Yau 1987). The major conclusion to be drawn is that our findings concerning the role of the ambient shear perpendicular to a slab-symmetric diabatic heating source are valid for a "bubble like" heating source.

6.3 Effects of the change of wind direction

This section deals with the effects of curvature in the ambient wind. Two experiments were made which had both non-zero U and non-zero V wind components. The U-profile in both cases was the same as given by Fig 5.2.1c but the V component varied with height according to Fig 6.3.1a and b, respectively. To capture the three dimensional structure of

the resulting updraft fields, we contour the vertical motion fields for three different vertical sections chosen at y = 45 km, 50 km and 55 km, respectively (Fig 6.3.2). The y = 50 km case shows the circulation in the vertical plane passing through the centre of the heating.

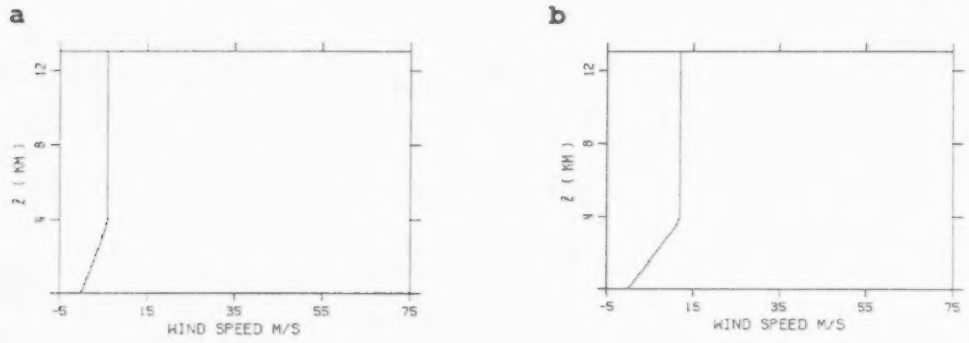

Figure 6.3.1 V component of the ambient wind.

Table 6.3.1 Vertical velocities and kinetic energies associated with directional shear.

Fig	W_{max}	W_{min}	KE_w	V_{4km}
6.1.2	6.4	-2.6	3.0	0
6.2.2a	6.5	-2.4	2.8	6
6.2.2b	7.8	-2.6	3.7	12

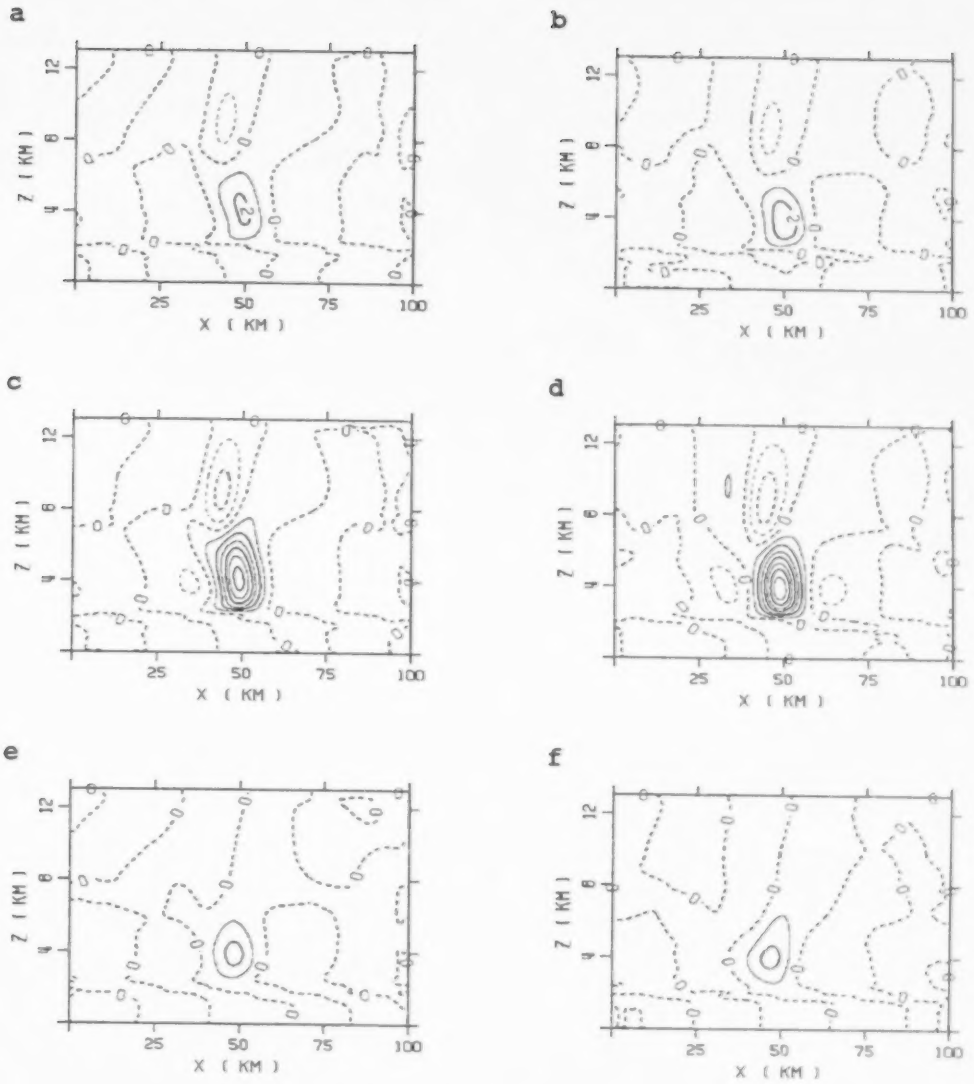

Fig 6.3.2 Vertical velocity fields for three dimensional "bubble like cell" in a directionally shear environment. (a),(b); y = 45 km, (c),(d); y = 50 km and (e),(f); y = 55 km represent cross-sections of the vertical motion field. V component of wind given in 6.3.1a used for (a), (c) and (e). V component of wind given in 6.3.1b used for (b), (d) and (f).

The results indicate some degree of asymmetric structure in that the fields at 45 and 55 km are <u>not</u> identical. The cells in the northerly plane y = 55 km are slightly deeper than those in the southerly plane due to the northerly advection of the heating which causes local buoyancy and updraft production. When the V component of the wind is larger (V=12 m s^{-1}), the convection became more intense. Comparison of the w_{max}, w_{min} and KE_w values confirm this behaviour (Table 6.3.1). In conclusion, we find that the shear amount (i.e. V-component) perpendicular to the main shear direction affects the circulation by creating an asymmetric vertical motion field and tends to enhance the peak updraft speed. Furthermore, a secondary circulation can develop both upwind and downwind of the core updraft (Fig 6.3.3). We note that the circular shape has been changed to a <u>sheared</u> ellipse with its major axis pointing northwestward perpendicular to the low level wind.

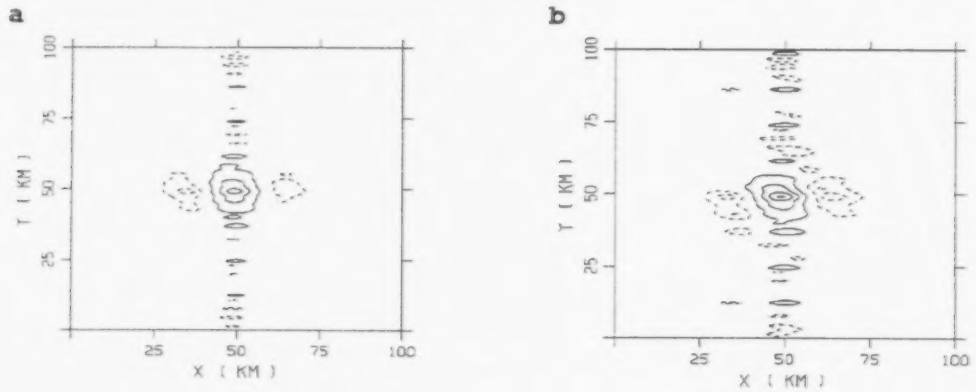

Fig 6.3.3 Horizontal section of the vertical motion fields associated with V component of wind given in fig 6.2.1a for (a) and V component of wind given in 6.2.1b for (b). Note the contour interval every 2 cm s^{-1} for positive values and every .5 cm s^{-1} for negative values.

7 Case Study

In this chapter we present an example of how the linear steady state model may be used to interpret mesoscale weather. We have examined sounding data from Stony Plain AB for the entire summer of 1991 and selected the day of 3 July 1991 for this case study.

The choice of particular day was based on the fact that the observed temperature and moisture profiles remained similar for the morning (0600 local time) and the evening (1800 local time). The average of the two temperature profiles is depicted in Fig 7.1. While the temperature varied by less then 1.5 C from the average profile (within the error of the instrumentation used), major changes were found in the wind structure (Fig 7.2). During the afternoon a strong upper level jet developed and also the lower level wind pattern changes.

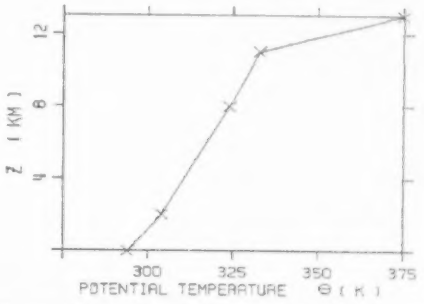

Figure 7.1 Average potential temperature profile for July 3, 1991

Synoptic conditions remained almost the same. An upper level low was situated over the Gulf of Alaska with a weak ridge over central Saskatchewan. Surface conditions indicated a weak low over the northeast corner of Alberta with a trough or weak frontal zone extending southwestward. While the atmospheric stability and the synoptic forcing were very similar, the observed mesoscale weather changed from isolated morning showers to afternoon scattered thundershowers. This significant change in the convective

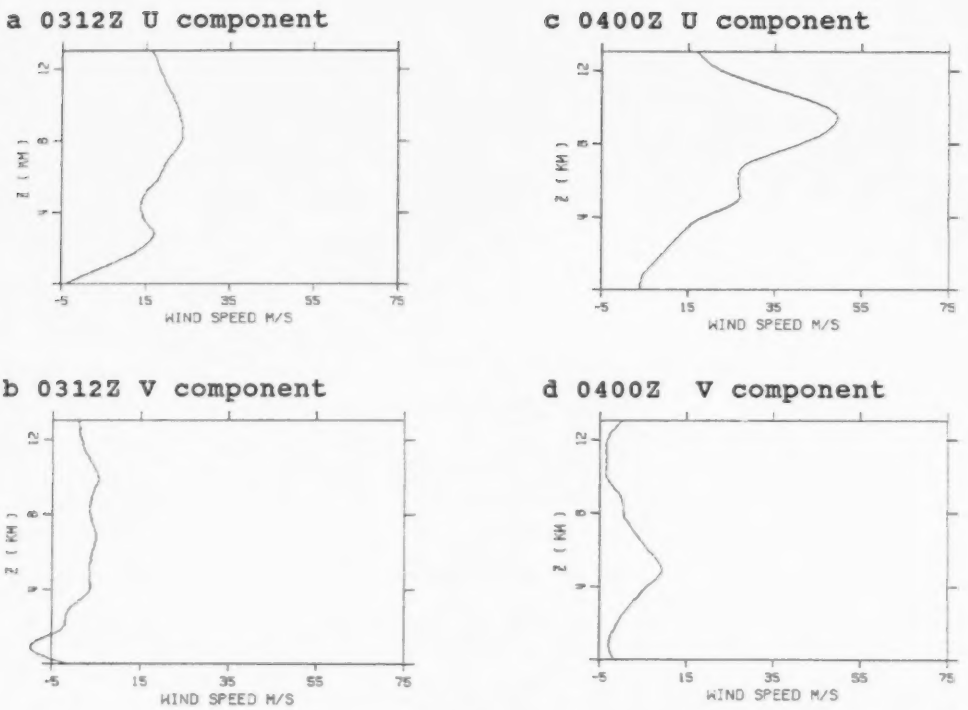

Figure 7.2 Morning and afternoon horizontal wind components

activity between the morning and afternoon may have been caused by several factors such as enhanced surface convergence, triggering by enhanced surface heating and interaction of the existing cloud clusters.

We will now use the model to examine whether the observed increase of wind shear could be partly responsible for the organization and intensity of the vertical motion field. The temperature profile (Fig 7.1) was used to

estimate the Brunt-Väisälä frequency as a function of height. The basic state wind was taken from the observed wind profiles. Both morning and evening cases have the same diabatic forcing to allow for easy comparison. Specifically, the heating term was identical to that used in the control case of chapter 5. The dissipation coefficient was taken to be 10^{-4} s^{-1} with a sponge layer at the surface and near the top of the model domain as described in chapter 4.

The numerical results indicate that the average kinetic energy and the peak updraft and downdraft speeds are more than twice as strong for the conditions in the evening, as compared to the morning wind conditions (Table 7.1). Fig 7.3 gives the vertical motion field at 5 km intervals away from the centre of the maximum heating rate. This is done to allow a three dimensional look at the vertical structure. The circulation for the evening case is much deeper than for the morning case. In fact, the morning case reveals that the vertical motion field does not even reach the top of the positive diabatic heating (8 km). Whereas, the afternoon case indicates the vertical motion field extending up to the tropopause (11 km). A comparison of the vertical motion fields associated with the afternoon case indicates the upstream downdraft 5 km south (Fig 7.3b) of the centre is much stronger than the downstream

Table 7.1 Comparison of peak vertical velocities and kinetic energies associated with case study

Units as per table 4.1.

Fig	7.4b	7.4d
W_{max}	18.3	36.4
W_{min}	-5.8	-17.9
KE_W	22	254
V_g	-1.5	1.1
U_g	13.2	8.1

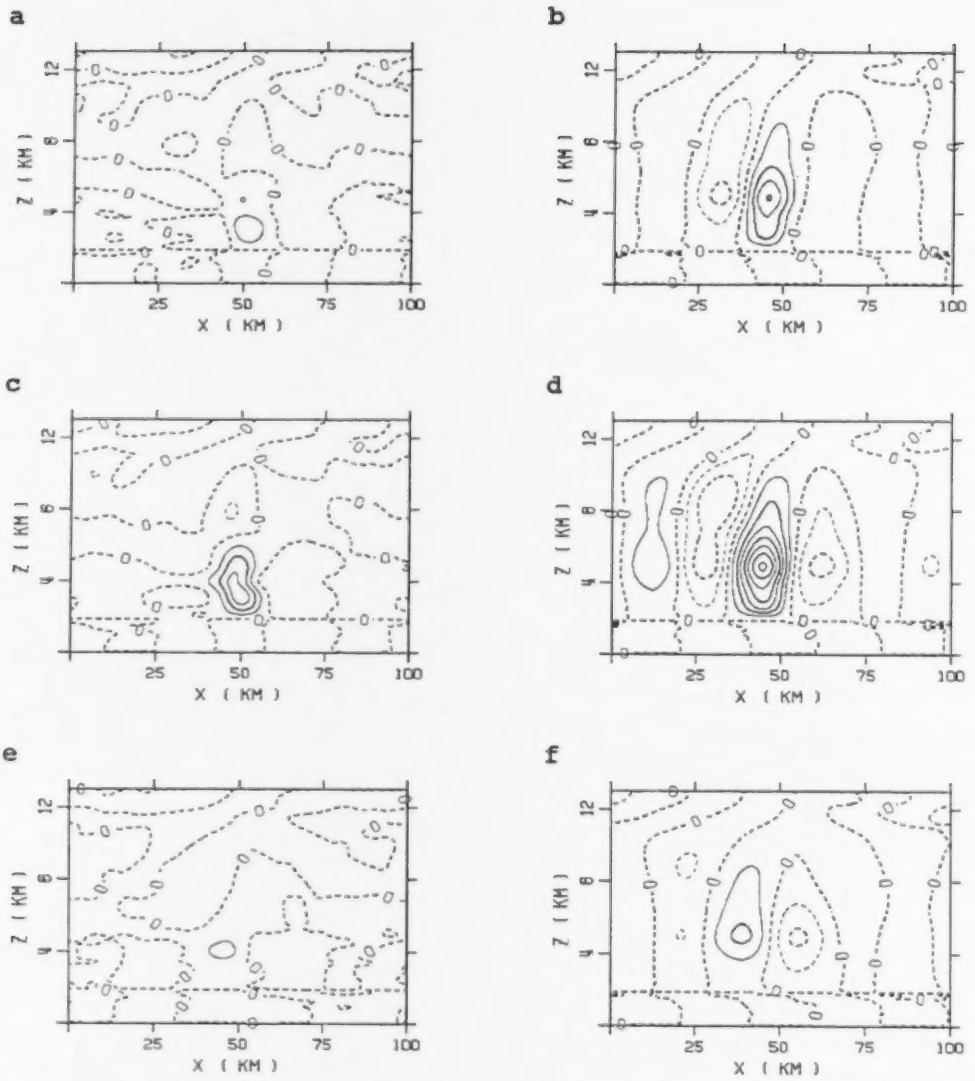

Fig 7.3 Three dimensional vertical motion fields for case study. (a) and (b); y = 45 km, (c) and (d); y = 50 km and (e) and (f); y = 55 km. Data for morning sounding used in (a), (c) and (e). Data for afternoon sounding used in (b), (d) and (f). Contour interval every 5 cm s^{-1}

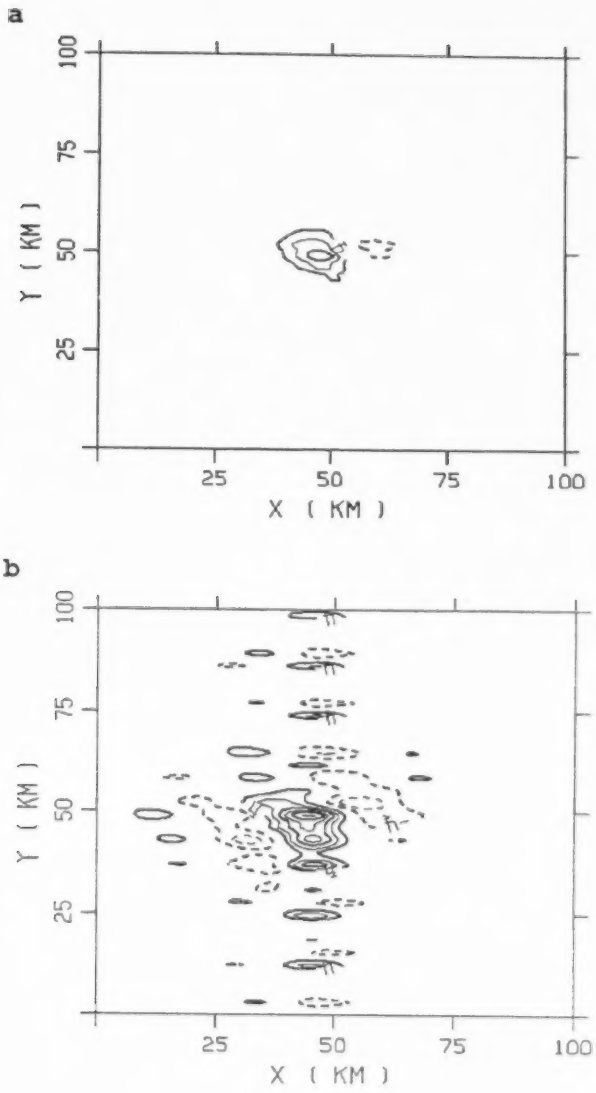

Fig 7.4 Horizontal section of vertical motion fields for morning (a) and afternoon (b) parameters. Note contour interval every 4 cm s^{-1} with no zero contour.

updraft, whereas the opposite is true for the downdraft 5 km north (Fig 7.3c). To investigate why this occurs it will be necessary to look at the horizontal vertical velocity fields. We choose the 4 km level since this is near the level of maximum updraft (Fig 7.3).

The horizontal depiction (Fig 7.4) gives the opportunity to look at the spatial distribution of vertical motion field. This depiction indicates the development of a northwest-southeast line of updrafts in the afternoon, as well as, a secondary line of updrafts both upstream and downstream (Fig 7.4b) in the same orientation. The northwest-southeast lines appear to be dependent on the three dimensional wind. Examination of the wind profile indicates that this line is perpendicular to the ambient wind at 4 km.

The development of secondary lines of updrafts, the increase in depth of the vertical motion field and the increase in strength of the vertical motion field are the results one would have expect given the observations for the day. It would appear that buoyancy waves were a contributing factor in the development of convective activity during the day.

The control case indicates that the buoyancy wave solution to the vertical motion field can provide valuable information on the development of convection and its spatial distribution. In order to investigate the true value of the model in terms of case studies many detailed comparisons of model and observational results would be needed. Since this section is intended to introduce the possible uses of the model in terms of studying convective activity, further study is left for further research.

8 Discussion and Conclusions

A two and three dimensional linearized buoyancy wave model has been used to investigate the effects of wind shear, diabatic heating, and atmospheric stability on the buoyancy wave contribution to the vertical motion field. The focus has been to study the effects of wind shear on the circulation.

Results show that certain model parameters effect the vertical motion fields by enhancing the magnitude of the peak vertical velocity, by changing the structure (i.e. the tilt of the vertical motion field) or both.

The magnitude of the wind shear, the static stability and the dissipation coefficient effect both the structure and the intensity of the vertical motion field. Specifically:

1) An increase in the magnitude of the shear increases the speed of the peak updraft. Furthermore, it also increases the upwind tilt of the updraft core in the lower troposphere. On the other hand, an increase in wind shear decreases the downwind tilt in the secondary updraft in the upper troposphere.

2) An increase in the static stability (i.e. decrease in the Brunt-Väisälä frequency) causes a significant increase in the speed of the peak updraft. Also the circulation becomes more erect.

3) An increase in the magnitude of the dissipation coefficient, decreases the intensity of the circulation and also makes the circulation more erect.

The following conditions seem to affect only the intensity of the circulation without effecting the structure:

4) The magnitude of the vertical velocity increases when the curvature (i.e. second derivative) of the ambient wind decreases provided the first derivative remains positive throughout the heating layer.

5) An increase in the diabatic heating rate, increases the strength of the vertical motion field.

One condition seems to have a rather small effect on the intensity of the updraft but largely determines it's structure:

6) Increasing the depth of the diabatic heating source, makes the circulation more erect.

Some of these finding are similar to those reported by Takeda (1974). His results were obtained using a time-dependent non-linear cumulus convective model. The agreement in results based on totally different numerical models, gives confidence that our linearized buoyancy wave model may be useful in identifying atmospheric conditions that contribute to the enhancement of the vertical motion field and thus to storm development. These conditions may help researcher to focus on the conditions which produce the environment necessary for storm development. Since the operation of a time dependent, three dimensional mesoscale model including a complex physics package requires extensive computer resources it may be possible to pinpoint the conditions necessary to enhance the vertical motion field, thus decreasing the number of model runs required by the full physics model.

In chapter 3 we identified four parameters necessary for

a strong updraft field. These parameters are defined by the relationship between the Scorer parameter (which is a function of the static stability, the ambient wind and the second derivative of the wind) and the dimensions of the convective cloud. As the value of the Scorer parameter approaches the wave number of the cloud dimensions the vertical motion field will be intensified. This seems consistent with previous studies. Byers and Braham (1949) indicated that strong wind shear has negative effect on the development of small cumuli (i.e. small value of the Scorer parameter associated with a large value in wave number). Weisman and Klemp (1982) indicated that large cumuli are enhance by strong wind shear (i.e. wave number of the dimensions of the cell approaching the value of the Scorer parameter).

The enhancement of the convective clouds associated with low level jets was investigated in chapter 5. We showed that the enhancement may be due to the enhanced buoyancy wave vertical motion field associated with a low level jet as defined in a moving frame of reference. This implies that a low level jet velocity which is opposite in direction to the ambient wind flow aloft is important to the development of a strong vertical motion field.

In chapter 5 we simulated the affect on the vertical vertical motion field as the Scorer parameter approaches the value of the wave number of the heating. We found that we could establish a enhanced vertical motion field associated with relatively weak wind shear conditions. It is likely that the relationship between the Scorer parameter and the dimensions of the convective cell are <u>not</u> independent (both are dependent on stability) of each other. It is left for further study to see if there exists a function that relates

the dimensions of the convective cell and the Scorer parameter.

The three dimensional model indicates that the combined effects of veering and sheer can produce an enhanced vertical motion field. With our computing resources consisting of a PC386 machine, only a few fully three-dimensional model runs have been made. We believe that interesting results can be obtained from experimenting with numerous wind hodographs. Future research, based on running the model on a workstation should identify the correctness of our speculation.

The case study indicated that this model could be a valuable tool in determining the parameters which will produce a strong vertical motion field and hence lead to storm development. By comparing the vertical motion fields derived from the morning and evening sounding, we found that the vertical motion field associated with the afternoon conditions was twice as strong compared to the vertical motion field associated with the morning. This lead to the conclusion that the convective activity would be enhanced in the afternoon due to gravity waves. This conclusion was verified by observation of increased convective activity (i.e. isolated morning showers; scattered afternoon thundershowers).

The primary goal of the thesis was to find a relationship between the updraft field and the diabatic heating rate, the ambient wind and the static stability. This should allow for the ability to better assimilate new wind measurements derived from Doppler radar and profilers. We find that a comparison between the size of the heating elements (i.e. convective clouds and estimated using

satellite imagery and radar) and the Scorer parameter (estimated using doppler radar and satellite sounding) may be a key to understanding the process of storm enhancement. As this new technology becomes available it is hoped that this relationship will provide meteorologists with an effective criterion which will increase the usefulness of this new data.

9 References

Bluestein, H.B. and M.H. Jain, 1985: Formation of mesoscale lines of precipitation: Severe squall lines in Oklahoma during the spring. Journal of the Atmospheric Sciences, Vol 42, pp 1711-1732.

Bonner, W.D., 1968: Climatology of the low level jet. Monthly Weather Review, Vol 96, pp 833-850.

Byers, H.R., and R.R. Braham, 1949: The thunderstorm. U.S. Department of Commerce.

Chisholm, A.J. and M. English, 1973: Alberta hailstorms. Meteorological Monogram, Vol 14, No. 36.

Cram, J.M., R.A. Pielke, W.R. Cotton, 1992: Numerical simulation and analysis of a prefrontal squall line. Part I: Observations and basic simulation results. Journal of the Atmospheric Sciences, Vol 49, pp 189-208.

Cram, J.M., R.A. Pielke, W.R. Cotton, 1992: Numerical simulation and analysis of a prefrontal squall line. Part II: Propagation of the squall line as an internal gravity wave. Journal of the Atmospheric Sciences, Vol 49, pp 209-225.

Crapper, G.D., 1959: A three-dimensional solution for waves in the lee of mountains. Journal of Fluid Mechanics, Vol 6, pp 51-76.

Durran, R.D. and J.B. Klemp, 1982: On the effects of moisture on the Brunt-Väisälä frequency. Journal of the Atmospheric Sciences, Vol 39, pp 2152-2158.

Durran, R.D. and J.B. Klemp, 1982: The effects of moisture on trapped mountain lee waves. Journal of the Atmospheric Sciences, Vol 39, pp 2490-2506.

Durran, R.D. and J.B. Klemp, 1983: A compressible model for the simulation of moist mountain waves. Monthly Weather Review, Vol 111, pp 2341-2361.

Emanual, K.A., 1986: Some dynamic aspects of precipitation convection. Journal of the Atmospheric Sciences, Vol 43, pp 2183-2198.

Fovell, R.G. and Y. Ogura, 1989: Effects of vertical wind shear on numerical simulated multicell storm structures. Journal of the Atmospheric Sciences, Vol 46, pp 3144-3176.

Gossard, E.E. and W.H. Hooke, 1975: Waves in the atmosphere. Developments in atmospheric science, 2. Elsevier Scientific Publishing Company, Amsterdam.

Holton, J.R., 1979: An introduction to dynamic meteorology. Academic Press.

Hoxit, L.R., 1975: Diurnal variations in planetary boundary-layer winds over land. Boundary layer Meteorology, Vol 8, pp 21-38.

Iribarne, J.V. and W.L. Godson, 1981: Atmospheric thermodynamics. D. Reidel Publishing Company.

Kaplan, M.L., J.W. Zack, V.C. Wong and J.J. Tuccillo, 1982: Initial results from MASS and comparison with AVE-Sesame I data set. Monthly Weather Review, Vol 110, pp 1564-1590.

Lin, Yuh-Lang and Hye-Yeong Chun, 1991: Effects of diabatic cooling in a shear flow with a critical level. Journal of the Atmospheric Sciences, Vol 48, pp 2476-2491.

Lin, Yuh-Lang and Shiaolin Li, 1988: Three dimensional response of a shear flow to elevated heating. Journal of the Atmospheric Sciences, Vol 45, pp 2987-3002.

Lin, Yuh-Lang, 1987: Two dimensional response of a stably stratified shear flow to diabatic heating. Journal of the Atmospheric Sciences, Vol 44, pp 1375-1393.

Lin, Yuh-Lang and R.B. Smith, 1986: Transient dynamics of airflow near a local heat source. Journal of the Atmospheric Sciences, Vol 43, pp 40-49.

Maddox, R.A., 1980: Mesoscale convective complexes. Bulletin of the American Meteorology Society, Vol 61, pp 1374-1387.

Mastrantonio, G., F. Einaudi, D. Fua, and D.P. Lalas, 1976:

Generation of gravity waves by jet streams in the atmosphere. Journal of the Atmospheric Sciences, Vol 33, pp 1730-1738.

Moncrieff, M.W., and J.S.A. Green, 1972: The propagation and transfer properties of steady convective overturning in shear. Quarterly Journal of the Royal Meteorological Society, Vol 98, pp 336-352.

Nastrum, G.D., M.R. Peterson, J.L. Green, K.S. Gage and T.E. VanZandt, 1990: Sources of gravity wave activity seen in the vertical velocities observed by the Flatland VHF radar. Journal of Applied Meteorology, Vol 29, pp 783-792.

Pastushkov, R.S. 1975: The effects of vertical wind shear on the evolution of convective clouds. Quarterly Journal of the Royal Meteorological Society, Vol 101, pp 281-292.

Raymond, D.J., 1984: A Wave-CISK model of squall lines. Journal of the Atmospheric Sciences, Vol 41, pp 1946-1958.

Raymond, D.J., 1986: Prescribed heating of a stratified atmosphere as a model for moist convection. Journal of the Atmospheric Sciences, Vol 43, pp 1101-1111.

Reuter, G.W. and M.K. Yau, 1987: Numerical modelling of cloud development in a sheared environment. Contributions to Atmospheric Physics, Vol 60, pp 65-80.

Robichaud, A. and C.A. Lin, 1991: The linear steady response of a stratified baroclinic atmosphere to elevated diabatic heating. Atmosphere-Ocean, Vol 29, pp 619-635.

Robichaud, A. and C.A. Lin, 1989: Simple models of diabatically forced meso scale circulations and mechanism for amplification. Journal of Geophysical Research, Vol 94, pp 3413-3426.

Rogers, R.R., 1979: A short course in cloud physics. Pergamon Press.

Rotunno, R., J.B. Klemp and M.L. Weisman, 1988: The theory of long-lived squall lines. Journal of the Atmospheric Sciences, Vol 45, pp 463-485.

Scorer, R.S., 1949: Theory of waves in the lee of mountains. Quarterly Journal of the Royal Meteorological Society, Vol 75, pp 41-56.

Smith, R.B., 1980: Linear theory of stratified hydrostatic flow past an isolated mountain. Tellus, 1980, pp 348-364.

Steiner J.T., 1973: A three-dimensional model of cumulus cloud development. Journal of the Atmospheric Sciences. Vol 30, pp 414-435.

Takeda T., 1971: Numerical simulation of a precipitating convective cloud: The formulation of a "Long-lasting" cloud. Journal of the Atmospheric Sciences. Vol 28, pp 350-376.

Uccellini, L.W., R.A. Petersen, K.F. Brill, P.J. Kocin and J.J. Tuccillo, 1987: Synergistic interaction between an upper-level jet streak and diabatic processes that influence the development of a low-level jet and a secondary coastal cyclone. Monthly Weather Review, Vol 115, pp 2227-2261.

Weisman, M.L., and J.B. Klemp, 1982: The dependence of numerically simulated convective storms on vertical wind shear and buoyancy. Monthly Weather Review, Vol 110, pp 504-520.

Wilhelmson, R.B., and J.B. Klemp, 1978: A numerical study of storm splitting that leads to long lived storms. Journal of the Atmospheric Sciences, Vol 35, pp 1974-1986.

Wilhelmson, R.B., and J.B. Klemp, 1981: A three-dimensional numerical simulation of splitting severe storms on 3 April 1964. Journal of the Atmospheric Sciences, Vol 38, pp 1581-1600.

Yanai, M., S. Esbensen, and J. Chu, 1973: Determination of bulk properties of tropical cloud clusters from large-scale heat and moisture Budgets. Journal of the Atmospheric Sciences, Vol 30, pp 611-627.

Appendix 1

Solution to governing equations in two dimensions

The governing linear equations of motion for a perturbation in an incompressible, stratified Boussinesq airflow with diabatic heating can be written as:

$$1)\ U\frac{\partial u}{\partial x} + w\frac{\partial U}{\partial z} + \frac{1}{\rho}\frac{\partial P}{\partial x} + \beta u = 0$$

$$2)\ U\frac{\partial w}{\partial x} + \frac{1}{\rho}\frac{\partial P}{\partial z} + g\frac{\varrho}{\rho} + \beta w = 0$$

$$3)\qquad \frac{\partial u}{\partial x} + \frac{\partial w}{\partial z} = 0$$

$$4)\ U\frac{\partial \varrho}{\partial x} - w\rho\frac{N^2}{g} + \beta\rho = -\frac{\rho}{CT}q$$

To eliminate P from equation 1 and 2

a) take the derivative with respect to z of equation 1 gives:

$$5)\ \frac{\partial U}{\partial z}\frac{\partial u}{\partial x} + U\frac{\partial^2 u}{\partial z \partial x} + \frac{\partial w}{\partial z}\frac{\partial U}{\partial z} + w\frac{\partial^2 U}{\partial z^2} + \frac{1}{\rho}\frac{\partial}{\partial z}\frac{\partial P}{\partial x} + \beta\frac{\partial u}{\partial z} = 0$$

b) take the derivative with respect to x of equation 2 gives:

$$6)\ U\frac{\partial^2 w}{\partial x^2} + \frac{1}{\rho}\frac{\partial}{\partial x}\frac{\partial P}{\partial z} + \frac{g}{\rho}\frac{\partial \varrho}{\partial x} + \beta\frac{\partial w}{\partial x} = 0$$

c) subtracting equations 5 and 6 gives:

$$7)\quad \frac{\partial U}{\partial z}\frac{\partial u}{\partial x}+U\frac{\partial^2 u}{\partial z\partial x}+\frac{\partial w}{\partial z}\frac{\partial U}{\partial z}+w\frac{\partial^2 U}{\partial z^2}+\beta\frac{\partial u}{\partial z}-U\frac{\partial^2 w}{\partial x^2}-\frac{g}{\rho}\frac{\partial \varrho}{\partial x}-\beta\frac{\partial w}{\partial x}=0$$

To eliminate ρ and ϱ from the equations:

a) take the second derivative with respect to x of equation 4 gives:

$$8)\quad U\frac{\partial^3 \varrho}{\partial x^3}-\frac{\rho N^2}{g}\frac{\partial^2 w}{\partial x^2}+\beta\frac{\partial^2 \varrho}{\partial x^2}=-\frac{\rho}{CT}\frac{\partial^2 q}{\partial x^2}$$

b) manipulate equation 7, eliminate u using equation 3 and take derivative with respect to x gives:

$$9)\quad \frac{\partial^2 \varrho}{\partial x^2}=\frac{\rho}{g}\left[-\left(U\frac{\partial}{\partial x}+\beta\right)\frac{\partial^2 w}{\partial z^2}+\frac{\partial}{\partial x}\left(\frac{\partial^2 U}{\partial z^2}w-U\frac{\partial^2 w}{\partial x^2}-\beta\frac{\partial w}{\partial x}\right)\right]$$

c) combining equation 9 and 8 gives:

$$10)\quad U\left[-\frac{\partial}{\partial x}\left(U\frac{\partial}{\partial x}+\beta\right)\frac{\partial^2 w}{\partial z^2}+\frac{\partial^2}{\partial x^2}\left(\frac{\partial^2 U}{\partial z^2}w-U\frac{\partial^2 w}{\partial x^2}-\beta\frac{\partial w}{\partial x}\right)\right]-N^2\frac{\partial^2 w}{\partial x^2}$$

$$+\beta\left[-\left(U\frac{\partial}{\partial x}+\beta\right)\frac{\partial^2 w}{\partial z^2}+\frac{\partial}{\partial x}\left(\frac{\partial^2 U}{\partial z^2}w-U\frac{\partial^2 w}{\partial x^2}-\beta\frac{\partial w}{\partial x}\right)\right]=-\frac{g}{CT}\frac{\partial^2 q}{\partial x^2}$$

Manipulation of equation 10 gives the equation in final form:

$$\left(U\frac{\partial}{\partial x}+\beta\right)^2\left(\frac{\partial^2 w}{\partial x^2}+\frac{\partial^2 w}{\partial z^2}\right)-\left(U\frac{\partial}{\partial x}+\beta\right)\left(\frac{\partial^2 U}{\partial z^2}\frac{\partial w}{\partial x}\right)+N^2\frac{\partial^2 w}{\partial x^2}=\frac{g}{CT}\frac{\partial^2 q}{\partial x^2}$$

Appendix 2

The three dimensional model in microsoft fortran code is presented below. The individual programs are run sequentially to ensure data files are available for the next step of the calculations.

```
C*********************************************************
C     PROGRAM WIND
C
C     PROGRAM IS DEVELOPED TO INPUT BASIC STATE WIND
C     VELOCITIES AND SECOND DERIVATIVE OF WIND FOR OTHER
C     PROGRAMS. ENTRY OF WINDS IS DONE ON A LEVEL TO LEVEL
C     BASIS WITH THE CURVATURE OF THE WIND IN EACH LAYER
C     CHOOSEN BY THE INDIVIDUAL.
C
      PARAMETER(N=52)
      INTEGER IZ
      REAL*8 U(52),GGU(52),V(52),GGV(52)
C
C...  CALCULATE THE WIND
C
      CALL SPEED (N,U,GGU,V,GGV)
C
C...  WRITE WINDS TO FILES.
C
      OPEN(1,FILE='WINDU')
      WRITE(1,10) (U(IZ),IZ=1,N)
10    FORMAT(F15.8,F15.8)
      OPEN(2,FILE='TRANS')
      WRITE(2,10) (GGU(IZ),IZ=1,N)
      OPEN(3,FILE='RELU')
      WRITE(3,10) (U(IZ),IZ=1,N)
      OPEN(4,FILE='WINDV')
      WRITE(4,10) (V(IZ),IZ=1,N)
      OPEN(5,FILE='RELV')
      WRITE(5,10) (V(IZ),IZ=1,N)
      OPEN(6,FILE='TRANSV')
      WRITE(6,10) (GGV(IZ),IZ=1,N)
      END
C
      SUBROUTINE SPEED(N,U,GGU,V,GGV)
C
C     SUBROUTINE TO CALCULATE WIND AT LEVEL OF THE
C     ATMOSPHERE STEADY STATE WIND PROFILE REQUIRED.
C
      INTEGER Z,N,LVL(20),M,J,SM,B
      REAL*8 X(52),U(52),GGU(52),MID(20),TEMPA,TEMPB,Y(52)
      REAL*8 V(52),GGV(52),TEMPC
```

```
C
C...  ENTER WINDS AT GIVEN LAYERS TO DESCRIBED VELOCITY
C     FIELD.
C
      DO 100 B=1,2
      IF (B .EQ. 1) THEN
      WRITE(*,*) 'ENTER U COMPONENT OF WIND'
      ELSE
      WRITE(*,*) 'ENTER V COMPONENT OF WIND'
      ENDIF
      LVL(1)=1
      WRITE(*,*) 'ENTER SURFACE WIND SPEED IN M/S'
      READ(*,*) MID(1)
      DO 50 I=2,20,2
      WRITE(*,*) 'WIND AT NEXT LEVEL'
      READ(*,*) MID(I+1)
      WRITE(*,*) 'HEIGHT OF NEXT LEVEL IN METERS'
      READ(*,*) LVL(I+1)
      LVL(I+1)=LVL(I+1)/250
      WRITE(*,*) 'DEPARTURE FROM STAIGHT LINE WIND'
      READ(*,*) MID(I)
      WRITE(*,*) 'LEVEL OF DEPARTURE'
      READ(*,*) LVL(I)
      LVL(I)=LVL(I)/250
      TEMPB=(MID(I+1)-MID(I-1))/(FLOAT(LVL(I+1)-LVL(I-1)))
      MID(I)=MID(I)+(MID(I-1)+(TEMPB*(LVL(I)-LVL(I-1))))
      M=I
      IF (LVL(I+1) .EQ. N) GOTO 60
50    CONTINUE
60    CONTINUE
C
C...  CALCULATE THE CONSTANTS FOR EACH LAYER.
C
      DO 95 J=2,M,2
      TEMPA=((MID(J)-MID(J-1))/(LVL(J)-LVL(J-1)))
      TEMPA=TEMPA-((MID(J+1)-MID(J))/(LVL(J+1)-LVL(J)))
      TEMPB=(LVL(J)**2-LVL(J-1)**2)/(LVL(J)-LVL(J-1))
      TEMPB=TEMPB-((LVL(J+1)**2-LVL(J)**2)
     1 /(LVL(J+1)-LVL(J)))
      TEMPC=TEMPA/TEMPB
      TEMPB=(MID(J)-MID(J-1))-
     1 ((LVL(J)**2-LVL(J-1)**2)*TEMPC)
      TEMPB=TEMPB/(LVL(J)-LVL(J-1))
      TEMPA=MID(J-1)-(LVL(J-1)*TEMPB)-((LVL(J-1)**2)*TEMPC)
C
C...   CALCULATE THE HORIZONTAL WIND AT EACH LAYER
C
      IF (B .EQ. 1) THEN
      DO 85 Z=LVL(J-1),LVL(J+1)
      U(Z)=TEMPA+(TEMPB*Z)+(TEMPC*(Z**2))
```

```
85     CONTINUE
       ELSE
       DO 90 Z=LVL(J-1),LVL(J+1)
       V(Z)=TEMPA+(TEMPB*Z)+(TEMPC*(Z**2))
90     CONTINUE
       ENDIF
95     CONTINUE
100    CONTINUE
C
C...  SMOOTH DATA TO REMOVE SINGULARITY
C
       WRITE(*,*)'NUMBER OF SMOOTHING REQUIRED'
       READ(*,*) SM
       DO 120 I=1,SM
       DO 110 Z=2,N-1
       Y(Z)=(.25*U(Z-1))+(.50*U(Z))+(.25*U(Z+1))
       X(Z)=(.25*V(Z-1))+(.50*V(Z))+(.25*V(Z+1))
110    CONTINUE
C
C...   REPLACE ORIGINAL DATA WITH SMOOTHED DATA.
C
       DO 120 Z=2,N-1
       U(Z)=Y(Z)
       V(Z)=X(Z)
120    CONTINUE
C
C...   CALCULATE SECOND DERIVATIVE USING CENTRE DIFFERENCING
C      SCHEME.
C
       DO 150 Z=2,N-1
       GGU(Z)=(U(Z+1)-(2*U(Z))+U(Z-1))/(250**2)
       GGV(Z)=(V(Z+1)-(2*V(Z))+V(Z-1))/(250**2)
150    CONTINUE
       GGU(1)=GGU(2)
       GGV(1)=GGV(2)
       GGU(N)=GGU(N-1)
       GGV(N)=GGV(N-1)
       RETURN
       END

C*************************************************************
C     PROGRAM HEATFFT.3D
C
C     HEATING TERM WILL BE DEFINED AS A BUBBLE LIKE STRUCTURE
C     IN THE CENTRE OF THE GRID
C          Q = q (B^2/(X^2+Y^2+B^2)SIN ( )
C
C     FAST FOURIER ROUTINE IS THEN USED TO TRANSFORM
C     HEATING TERM INTO FOURIER SPACE.
C
```

```
C*************************************************************
      PARAMETER(NX=64,NY=64,N=52)
      REAL*8 WI(128,64),B,QI,DX,DY,WYI(64,128),HI,BASE,TOP
      REAL*8 FACTA,FACTB,FACTC,FACTD,FACTE,FACTF,PIE
      INTEGER IX,IZ
C
C... HALF WIDTH OF HEATING TERM
C
      B=5.0
C
C... ENTER MAXIMUM HEATING RATE.
C
      WRITE(*,*) ' ENTER HEATING TERM '
      READ (*,*) QI
C
C... SET BASE AND TOP OF POSITIVE HEATING RATE.
C
      WRITE (*,*) 'ENTER BASE AND TOP'
      READ(*,*) BASE,TOP
      BASE=BASE/250
      TOP=TOP/250
C
C... CALCULATE HEATING RATE OVER GRID IN REAL SPACE
C
      PIE=3.14
      FACTA = PIE*(0.5-(1.0/(BASE-1)))
      FACTB = PIE/(BASE-1)
      FACTC = PIE*(1.5-(BASE/(TOP-BASE)))
      FACTD = PIE/(TOP-BASE)
      FACTE = PIE*(2.5-(TOP/(48-TOP)))
      FACTF = PIE/(48-TOP)
      OPEN(7,FILE='QTERM')
      DO 5 IZ=1,N
      IF (IZ .LT. BASE) THEN
      HI=0.10*COS(FACTA+(FACTB*IZ))
      ELSE
      IF (IZ .LT. TOP) THEN
      HI=COS(FACTC+(FACTD*IZ))
      ELSE
      IF (IZ .LT. 48) THEN
      HI=0.05*COS(FACTE+(FACTF*IZ))
      ELSE
      HI=0.00
      ENDIF
      ENDIF
      ENDIF
      DO 10 IY=1,NY
      IF (IY .GT. 32) THEN
      DY= FLOAT(IY)-32.0
      ELSE
```

```
      DY= 32-FLOAT(IY)
      ENDIF
      DO 10 IX=2,NX*2,2
      WI(IX,IY)=0.0
      IF (IX .GT. 64) THEN
      DX= (FLOAT(IX)/2)-32
      ELSE
      DX= 32-(FLOAT(IX)/2)
      ENDIF
      WI(IX-1,IY)=HI*(QI/(((DX**2+DY**2)/(B**2))+1))
      WI(IX-1,IY)=WI(IX-1,IY)*SIN((FLOAT(IX)/12.8)*3.14)
      WI(IX-1,IY)=WI(IX-1,IY)*SIN((FLOAT(IY)/12.8)*3.14)
      IF (IZ .EQ. BASE) WI(IX-1,IY)=0.0
      IF (IZ .EQ. BASE+1) WI(IX-1,IY)=0.0
      IF (IZ .EQ. BASE-1) WI(IX-1,IY)=0.0
10    CONTINUE
C
C...  TRANSFORM HEATING TERM TO FOURIER SPACE
C
      CALL FOURA(NX,NY,WI,WYI)
C
C...  WRITE RESULTS TO FILE
C
      WRITE(7,6) ((WYI(IX,IY),IX=1,NX),IY=1,NY*2)
5     CONTINUE
6     FORMAT(F24.8,F24.8,F24.8)
      END
C
C
      SUBROUTINE FOURA(NX,NY,WI,WYI)
C
C...  FAST FOURIER TRANSFORM USED TO TRANSFORM HEATING TERM
C     INTO FOURIER SPACE.
C
      REAL*8 WR,WW,WPR,WPI,THETA,TEMPR,WI(128,64)
      REAL*8 WTEMP,TEMPI,WYI(64,128)
      INTEGER NX,S,T,NN,I,J,NMAX,M,ISIGN,Y
C
      ISIGN=1
      DO 400 Y=1,NY
      NN=2*NX
      J=1
      DO 100 I=1,NN,2
      IF (J.GT.I) THEN
      TEMPR=WI(J,Y)
      TEMPI=WI(J+1,Y)
      WI(J,Y)=WI(I,Y)
      WI(J+1,Y)=WI(I+1,Y)
      WI(I,Y)=TEMPR
      WI(I+1,Y)=TEMPI
```

```
      ENDIF
      M=NN/2
1     IF ((M.GE.2).AND.(J.GT.M)) THEN
      J=J-M
      M=M/2
      GO TO 1
      ENDIF
      J=J+M
100   CONTINUE
      NMAX=2
2     IF (NN.GT.NMAX) THEN
      ISTEP=2*NMAX
      THETA=6.2831853/(ISIGN*NMAX)
      WPR=-2.D0*DSIN(0.5D0*THETA)**2
      WPI=DSIN(THETA)
      WR=1.D0
      WW=0.D0
      DO 300 M=1,NMAX,2
      DO 200 I=M,NN,ISTEP
      J=I+NMAX
      TEMPR=SNGL(WR)*WI(J,Y)-SNGL(WW)*WI(J+1,Y)
      TEMPI=SNGL(WR)*WI(J+1,Y)+SNGL(WW)*WI(J,Y)
      WI(J,Y)=WI(I,Y)-TEMPR
      WI(J+1,Y)=WI(I+1,Y)-TEMPI
      WI(I,Y)=WI(I,Y)+TEMPR
      WI(I+1,Y)=WI(I+1,Y)+TEMPI
200   CONTINUE
      WTEMP=WR
      WR=WR*WPR-WW*WPI+WR
      WW=WW*WPR+WTEMP*WPI+WW
300   CONTINUE
      NMAX=ISTEP
      GO TO 2
      ENDIF
400   CONTINUE
      T=1
      DO 460 Y=1,NY*2,2
      S=1
      DO 470 I=1,NX
      WYI(I,Y)=WI(S,T)
      WYI(I,Y+1)=WI(S+1,T)
      S=S+2
470   CONTINUE
      T=T+1
460   CONTINUE
      DO 900 I=1,NX
      NN=2*NY
      J=1
      DO 500 Y=1,NN,2
      IF (J.GT.Y) THEN
```

```
      TEMPR=WYI(I,J)
      TEMPI=WYI(I,J+1)
      WYI(I,J)=WYI(I,Y)
      WYI(I,J+1)=WYI(I,Y+1)
      WYI(I,Y)=TEMPR
      WYI(I,Y+1)=TEMPI
      ENDIF
      M=NN/2
3     IF ((M.GE.2).AND.(J.GT.M)) THEN
      J=J-M
      M=M/2
      GO TO 3
      ENDIF
      J=J+M
500   CONTINUE
      NMAX=2
4     IF (NN.GT.NMAX) THEN
      ISTEP=2*NMAX
      THETA=6.2831853/(ISIGN*NMAX)
      WPR=-2.D0*DSIN(0.5D0*THETA)**2
      WPI=DSIN(THETA)
      WR=1.D0
      WW=0.D0
      DO 700 M=1,NMAX,2
      DO 600 Y=M,NN,ISTEP
      J=Y+NMAX
      TEMPR=SNGL(WR)*WYI(I,J)-SNGL(WW)*WYI(I,J+1)
      TEMPI=SNGL(WR)*WYI(I,J+1)+SNGL(WW)*WYI(I,J)
      WYI(I,J)=WYI(I,Y)-TEMPR
      WYI(I,J+1)=WYI(I,Y+1)-TEMPI
      WYI(I,Y)=WYI(I,Y)+TEMPR
      WYI(I,Y+1)=WYI(I,Y+1)+TEMPI
600   CONTINUE
      WTEMP=WR
      WR=WR*WPR-WW*WPI+WR
      WW=WW*WPR+WTEMP*WPI+WW
700   CONTINUE
      NMAX=ISTEP
      GO TO 4
      ENDIF
900   CONTINUE
      RETURN
      END

C*************************************************************
C     PROGRAM CONST.3D
C
C    PROGRAM IS DEVELOPED TO CALCULATE CONSTANT IN VERTICAL
C     VELOCITY EQUATION. USING METHODS SIMILIAR TO THAT
C    DEVELOPED BY LIN AND LI.(1982). VERTICAL VELOCITIES ARE
```

```
C     CALCULATED IN FOURIER SPACE FROM GOVERNING EQUATIONS.
C*************************************************************
      PARAMETER(NX=64,NY=64,N=52)
      INTEGER IX,Z,IY
      REAL*8 U(52),GGU(52),V(52),GGV(52),CORN(52)
      REAL*8 K(64),P(64,128),BRUNT(52),TEMP(52)
C
C
C...  READ IN WINDS FROM FILE
C
      OPEN (1,FILE='WINDU')
      READ (1,10) (U(Z),Z=1,N)
      CLOSE(1)
      OPEN (2,FILE='WINDV')
      READ (2,10) (V(Z),Z=1,N)
      CLOSE(2)
C
C...  READ IN GRADIENT OF WIND SHEAR FROM FILE
C
      OPEN (3,FILE='TRANS')
      READ (3,10) (GGU(Z),Z=1,N)
      OPEN (4,FILE='TRANSV')
      READ (4,10) (GGV(Z),Z=1,N)
10    FORMAT(F15.8,F15.8)
C
C...  CALCULATE WAVE NUMBERS AND WINDS IN FRAME OF REFERENCE
C
      CALL NUMBER(K,U,V,CORN,TEMP,BRUNT,N,NX)
C
C...  OUTPUT VALUES OF WAVE NUMBERS USED.
C
      OPEN(6,FILE='KTRANS')
      WRITE(6,30) (K(IX),IX=1,NX)
30    FORMAT(F15.8)
C
C...  INPUT WIND VALUES IN FRAME OF REFERENCE USED.
C
      OPEN (1,FILE='WINDU')
      WRITE (1,10) (U(IX),IX=1,N)
      OPEN (2,FILE='WINDV')
      WRITE (2,10) (V(IX),IX=1,N)
C
C...  CALCULATE CONSTANTS
      OPEN (8,FILE='OUTPUT')
C
32    FORMAT(F30.8)
      DO 35 Z=1,N
      CALL CALC (K,U(Z),V(Z),P,GGU(Z),GGV(Z),NX,NY,
     1 CORN(Z),BRUNT(Z))
      WRITE (8,32) ((P(IX,IY),IX=1,NX),IY=1,NY*2)
```

```
35    CONTINUE
      END
C*************************************************************
C
      SUBROUTINE NUMBER (K,U,V,CORN,TEMP,BRUNT,N,NX)
C
      INTEGER I,M,NX,N,RE,LX,NEXT,SFC,MOTION
      REAL*8 K(64),U(52),CORN(52),BR,TEMP(52)
      REAL*8 BRUNT(52),DX,LYR,BASE,SPDCLD,V(52),SPDV
C
C...  ENTER BASE OF CLOUD TO GIVE MOTION OF HEATING TERM
C     WITH RESPECT TO AXIS.
C
      WRITE(*,*) 'ENTER CLOUD BASE'
      READ(*,*) BASE
      MOTION=FLOAT (BASE/250)
C
C...  SUBTRACT CLOUD MOTION FROM WIND SPEED.
C
      SPDCLD=U(MOTION)
      SPDV=V(MOTION)
      DO 40 I=1,N
      U(I)=U(I)-SPDCLD
      V(I)=V(I)-SPDV
40    CONTINUE
C
C...  CALCULATE VAISALLA-BRUNT FREQUENCY AND TEMPERATURE AT
C     THE GRID LEVELS. PROGRAM CAN CALCULATE CONSTANT VALUES
C     FOR FOUR DIFFERENT LAYERS IN ATMOSPHERE AND A VARIABLE
C     FREQUENCY ADJUSTED FOR MOISTURE PRESENT IN THE HEATED
C     LAYER.
C
      WRITE(*,*)'WOULD YOU LIKE VARIABLE FREQUENCY,1=YES,
     1 0=NO '
      READ (*,*) RE
      WRITE(*,*) 'ENTER SURFACE VAISALLA-BRUNT FREQUENCY'
      READ(*,*) BR
      WRITE(*,*) 'ENTER HIEGHT IN METERS OF SURFACE
     1  FREQUENCY'
      READ(*,*) SFC
      SFC=SFC/250
      WRITE (*,*)'ENTER SURFACE TEMPERATURE IN KELVIN'
      READ(*,*) TEMP(1)
      WRITE(*,*)'ENTER TEMPERATURE AT TOP SURFACE FREQUENCY'
      READ(*,*) TEMP(SFC)
      DO 1 J=2,SFC-1
      TEMP(J)=TEMP(1)-(((TEMP(1)-TEMP(SFC))/FLOAT(SFC-1))
     1 *FLOAT(J-1))
1     CONTINUE
      DO 2 I=1,SFC
```

```
      BRUNT(I)=BR
2     CONTINUE
      WRITE(*,*)'ENTER SECOND (moist) LAYER FREQUENCY'
      READ(*,*) BR
      LX=SFC+1
      WRITE(*,*)'ENTER HEIGHT IN METERS OF SECOND LAYER'
      READ(*,*) NEXT
      NEXT=NEXT/250
      WRITE(*,*) ' ENTER TEMPERATURE AT TOP OF LAYER'
      READ(*,*) TEMP(NEXT)
      LYR=(TEMP(SFC)-TEMP(NEXT))/FLOAT(NEXT-SFC)
      DO 110 J=LX,NEXT-1
      TEMP(J)=TEMP(SFC)-(LYR*FLOAT(J-SFC))
110   CONTINUE
      IF (RE .EQ. 1) THEN
      DO 3 I=LX,NEXT
      IF (TEMP(I) .GT. 238) THEN
      BRUNT(I)=(BR**2)-((TEMP(I)-238)/450000.0)
      IF (BRUNT(I) .LT. 0) THEN
      BRUNT(I)=0
      ENDIF
      BRUNT(I)=BRUNT(I)**.5
      ELSE
      BRUNT(I)=BR
      ENDIF
3     CONTINUE
      ELSE
      DO 4 I=LX,NEXT
      BRUNT(I)=BR
4     CONTINUE
      ENDIF
      WRITE(*,*) 'ENTER THIRD LAYER FREQUENCY'
      READ(*,*) BR
      WRITE(*,*)'ENTER HEIGHT OF TROPOPAUSE'
      READ(*,*) LX
      LX=LX/250
      WRITE(*,*)'ENTER TROPOPAUSE TEMPERATURE'
      READ(*,*) TEMP(LX)
      LYR=(TEMP(NEXT)-TEMP(LX))/FLOAT(LX-NEXT)
      DO 111 J=NEXT+1,LX-1
      TEMP(J)=TEMP(NEXT)-(LYR*FLOAT(J-NEXT))
111   CONTINUE
      DO 5 I=NEXT+1,LX
      BRUNT(I)=BR
5     CONTINUE
      WRITE(*,*)'ENTER TEMPERATURE AT TOP'
      READ(*,*) TEMP(N)
      LYR=(TEMP(NEXT)-TEMP(N))/FLOAT(N-NEXT)
      DO 114 J=NEXT+1,N-1
      TEMP(J)=TEMP(NEXT)-(LYR*FLOAT(J-NEXT))
```

```
114    CONTINUE
       WRITE(*,*)'ENTER FREQUENCY FOR TOP LAYER'
       READ(*,*) BR
       DO 6 I=LX+1,N
       BRUNT(I)=BR
6      CONTINUE
C
C...   CALCULATE COEFFICIENT OF RAYLEIGH HEATING AND NEWTON
C      COOLING IN VERTICAL. ADJUSTMENT MADE TO INCREASE
C     COEFFICIENT IN THE SURFACE TO 1 KM LAYER AND THE LAYER
C      BETWEEN 11 AND 13 KM TO ENSURE CONSISTENTENCY OF
C      BOUNDARY CONDITIONS OF THE VERTICAL VELOCITY SET TO
C      ZERO.
C
       DO 7 I=1,N
       CORN(I)=.0001
7      CONTINUE
       DO 8 I=1,4
       CORN(I)=CORN(I)*(1+
      1 (4*(SIN(1.57*((FLOAT(4-I)/3)))))**2)
8      CONTINUE0
       DO 9 I=44,N
       CORN(I)=CORN(I)*(1+(4*(SIN(1.57*
      1 ((FLOAT(I-44)/(N-44))))))**2)
9      CONTINUE
C
C...   CALCULATE WAVE NUMBERS.
C
       M=NX/2
       DX=1562.5
       DO 400 I=1,M
       K(I)=6.283185*I/(NX*DX)
400    CONTINUE
C
        DO 410 I=M+1,NX
        K(I)=-6.283185*(NX+1.0-I)/(NX*DX)
410     CONTINUE
C
C...   WRITE VERTICAL TEMPERATURE DATA TO FILE.
C
       OPEN(5,FILE='TEMPER')
       WRITE(5,60) (TEMP(I),I=1,N)
60     FORMAT(F15.8)
       WRITE(*,*)'SPEED OF HEAT SOURCE = ',SPDCLD
       RETURN
       END
C*************************************************************
C
       SUBROUTINE CALC (K,UI,VI,P,GU,GV,NX,NY,CN,BT)
C
```

```
C     CALCULATE WAVE NUMBERS AND CONSTANT NEEDED TO
C     CALCULATE VERTICAL VELOCITIES IN FOURIER SPACE.
C
C     WAVE NUMBERS CALCULATED AS DESCRIBED IN SMITH 1980.
C
C    ADJUST WIND SPEEDS TO SPEED WITHIN FRAME OF REFERENCE.
C
C*************************************************************
      INTEGER JX,Y
      REAL*8 K(64),UI,TEMPA,TEMPB,P(64,128),CN
      REAL*8 BT,GU,TEMPC,COM,H,GV,VI
C
C...  ENTER CONSTANT OF GRID.
C
      H=250.00**2
C
C...  CALCULATE TWO DIMENSIONAL ARRAY OF CONSTANTS REQUIRED
C     TO SOLVE VERTICAL VELOCITY EQUATION IN FOURIER SPACE.
C
      BT=BT**2
      DO 420 JY=1,NY
      Y=JY*2
      DO 420 JX=1,NX
      COM=K(JX)*UI+K(JY)*VI
      TEMPA=-((K(JX)*GU+K(JY)*GV)*COM)/(COM**2+CN**2)
      TEMPB=BT*(COM**2-CN**2)/((COM**2+CN**2)**2)
      TEMPC=(TEMPB-1)*(K(JX)**2+K(JY)**2)
      P(JX,Y-1)=(TEMPA+TEMPC)*H
      TEMPA=-((K(JX)*GU+K(JY)*GV)*CN)/(COM**2+CN**2)
      TEMPB=(BT*(2*COM*CN))/((COM**2+CN**2)**2)
      TEMPC=TEMPB*(K(JX)**2+K(JY)**2)
      P(JX,Y)=(TEMPA+TEMPC)*H
420   CONTINUE
      RETURN
      END

C
C    PROGRAM CONHEAT3D
C
C    PROGRAM IS DEVELOPED TO CALCULATE CONSTANTS NEEDED
C    TO CALCULATE THE VERTICAL VELOCITIES IN THE
C    ATMOSPHERE USING EQUATION SIMILIAR TO THAT DEVELOPED
C    BY LIN AND LI (1982). FOR FURTHER CONSTANTS REFER TO
C    PROGRAM CONST
C
      PARAMETER(NX=64,NY=64,N=52)
      INTEGER IX,I
      REAL*8 U(52),V(52),CORN(52),T(52)
      REAL*8 K(64),Q(64,128),QI(64,128)
C
```

```
C...  READ IN NECESSARY DATA.
C
C...  HORIZONTAL WIND IN FRAME OF REFERENCE CALCUALATED
C     IN CONST.FOR
C
      OPEN (1,FILE='WINDU')
      READ (1,10) (U(I),I=1,N)
      OPEN (2,FILE='WINDV')
      READ (2,10) (V(I),I=1,N)
10    FORMAT(F15.8,F15.8)
C
C...  WAVE NUMBERS CALCULATED IN CONST.FOR
C
      OPEN (4,FILE='KTRANS')
      READ (4,11) (K(IX),IX=1,NX)
11    FORMAT(F15.8)
C
C...  HEATING RATE WITHIN GRID. CALCULATED IN HEATFFT.FOR
C
      DO 1 I=1,N
      CORN(I)=.0001
1     CONTINUE
C     BUFFER LEVEL TO LIMIT REFLECTION OF WAVES
      DO 2 I=1,4
      CORN(I)= CORN(I)*(1+(4*
     1 (SIN(1.57*((FLOAT(4-I)/3)))))**2)
2     CONTINUE
      DO 3 I=44,N
      CORN(I)=CORN(I)*
     1 (1+(4*(SIN(1.57*((FLOAT(I-44)/(N-44))))))**2)
3     CONTINUE
C
C...  READ IN VERTICAL TEMPERATURE PROFILE CALCULATED IN
C     PROGRAM CONST.
C
      OPEN(6,FILE='TEMPER')
      READ (6,11) (T(I),I=1,N)
C
      OPEN (7,FILE='QTERM')
C
C...  READ THE DATA DO THE CALCULATIONS
      OPEN(8,FILE='INPUT')
C
      DO 100 IZ=1,N
      READ (7,20) ((QI(IX,IY),IX=1,NX),IY=1,NY*2)
C
C...  CALCULATE CONSTANTS REQUIRED OVER GRID.
C
      CALL FORCE (IZ,Q,QI,NX,NY,K,U,V,CORN,T)
C
```

```
C...  WRITE CONSTANTS TO FILE
C
      WRITE(8,30) ((Q(IX,IY),IX=1,NX),IY=1,NY*2)
100   CONTINUE
20    FORMAT(F24.8,F24.8,F24.8)
30    FORMAT(F30.8)
      END
C
      SUBROUTINE FORCE(IZ,Q,QI,NX,NY,K,U,V,CORN,T)
C
C
      REAL*8 Q(64,128),QI(64,128),GRAV,T(52),CP
      REAL*8 K(64),U(52),V(52),H,TEMPF,TEMPD,CORN(52)
      INTEGER NX,JX,Y,IZ
C
C...  INPUT GRID SPECIFICATIONS
C
      H=250.00**2
C
C...  ENTER UNIVERSAL CONSTANTS
C
      GRAV=9.80665
      CP=1005.0000
C
C...  BEGIN CALCULATING CONSTANTS.
C
      DO 520 JY=1,NY
      DO 520 JX=1,NX
      Y=2*JY
      COM=K(JX)*U(IZ)+K(JY)*V(IZ)
      TEMPD=(GRAV*(K(JX)**2+K(JY)**2))/(CP*T(IZ))
      TEMPE=(COM**2-CORN(IZ)**2)/((COM**2+CORN(IZ)**2)**2)
      TEMPF=(2*COM*CORN(IZ))/((COM**2+CORN(IZ)**2)**2)
      Q(JX,Y-1)=((QI(JX,Y-1)*TEMPE)-
     1   (QI(JX,Y)*TEMPF))*TEMPD*H
      Q(JX,Y)=((QI(JX,Y-1)*TEMPF)+(QI(JX,Y)*TEMPE))*TEMPD*H
520   CONTINUE
      RETURN
      END

C
C     PROGRAM FOURSP3D
C
C     PROGRAM IS DEVELOPED TO CALCULATE VERTICAL VELOCITIES
C    FROM CONSTANTS CALCULATED IN PROGRAMS CONST AND CONHEAT
C     IN FOURIER SPACE AND WRITE OUT VALUES TO FILE.
C
      PARAMETER(NX=64,NY=64,N=52)
      INTEGER IX,IZ,IY,L
      REAL*8 P(128,52),Q(128,52),JUNK(128)
```

```
C
C...  READ IN CONSTANTS OBTAINED IN PROGRAM CONST.
C
10    FORMAT(F30.8)
      DO 150 L=1,NY
      OPEN (3,FILE='OUTPUT')
      OPEN (6,FILE='INPUT')
      WRITE(*,*) 'COMPLETE SOLUTION ',L
      DO 50 IZ=1,N
      DO 40 IY=1,NY
      IF (IY .EQ. L) THEN
      READ (3,10) (P(IX,IZ),IX=1,NX*2,2)
      READ (3,10) (P(IX,IZ),IX=2,NX*2,2)
      READ (6,10) (Q(IX,IZ),IX=1,NX*2,2)
      READ (6,10) (Q(IX,IZ),IX=2,NX*2,2)
      ELSE
      READ (3,10) (JUNK(IX),IX=1,NX*2)
      READ (6,10) (JUNK(IX),IX=1,NX*2)
      ENDIF
40    CONTINUE
50    CONTINUE
      CLOSE (3)
      CLOSE (6)
C
C...  CALCULATE VERTICAL VELOCITY FEILD IN FOURIER SPACE.
C
      CALL FOURSP (NX,N,P,Q)
C
C...  WRITE RESULTS TO FILE.
C
      OPEN(7,FILE='RESULTS')
      WRITE(7,10) ((P(IX,IZ),IX=1,NX*2),IZ=1,N)
150   CONTINUE
      END
C
C
      SUBROUTINE FOURSP(NX,N,P,Q)
C
C     CALCULATE VERTICAL VELOCITIES IN FOURIER SPACE
C
      INTEGER NX,JK,JZ,K,N
      REAL*8 P(128,52),TMPA,RTMPB(52),IMTMPB(52),RTMPC(52)
      REAL*8 IMTMPC(52),Q(128,52),TMP
C
      DO 600 JK=1,NX
      K=2*JK
      RTMPB(1)=P(K-1,1)-2
      IMTMPB(1)=P(K,1)
      RTMPC(1)=Q(K-1,1)
      IMTMPC(1)=Q(K,1)
```

```
      DO 610 JZ=2,N
      TMPA=P(K-1,JZ)-2
      TMP=RTMPB(JZ-1)**2+IMTMPB(JZ-1)**2
      RTMPB(JZ)=TMPA-(RTMPB(JZ-1)/TMP)
      IMTMPB(JZ)=P(K,JZ)+(IMTMPB(JZ-1)/TMP)
      RTMPC(JZ)=Q(K-1,JZ)-(RTMPB(JZ-1)*RTMPC(JZ-1)/TMP)
      RTMPC(JZ)=RTMPC(JZ)-(IMTMPB(JZ-1)*IMTMPC(JZ-1)/TMP)
      IMTMPC(JZ)=Q(K,JZ)+(IMTMPB(JZ-1)*RTMPC(JZ-1)/TMP)
      IMTMPC(JZ)=IMTMPC(JZ)-(RTMPB(JZ-1)*IMTMPC(JZ-1)/TMP)
610   CONTINUE
      TMP=RTMPB(N)**2+IMTMPB(N)**2
      P(K-1,N)=((RTMPC(N)*RTMPB(N))+
     1 (IMTMPC(N)*IMTMPB(N)))/TMP
      P(K,N)=((IMTMPC(N)*RTMPB(N))-(RTMPC(N)*IMTMPB(N)))/TMP
      DO 630 JZ=N-1,1,-1
      TMP=RTMPB(JZ)**2+IMTMPB(JZ)**2
      P(K-1,JZ)=(-P(K-1,JZ+1)*RTMPB(JZ))
     1 -(IMTMPB(JZ)*P(K,JZ+1))
      P(K-1,JZ)=P(K-1,JZ)+(RTMPC(JZ)*RTMPB(JZ))+
     1 (IMTMPC(JZ)*IMTMPB(JZ))
      P(K-1,JZ)=P(K-1,JZ)/TMP
      P(K,JZ)=(-P(K,JZ+1)*RTMPB(JZ))+(P(K-1,JZ)*IMTMPB(JZ))
      P(K,JZ)=P(K,JZ)-(RTMPC(JZ)*
     1 IMTMPB(JZ))+(IMTMPC(JZ)*RTMPB(JZ))
      P(K,JZ)=P(K,JZ)/TMP
630   CONTINUE
600   CONTINUE
      RETURN
      END

C
C     PROGRAM FFT-3D
C
C     FAST FOURIER ROUTINE TO TRANSFORM VERTICAL VELOCITIES
C     CALCULATED IN FOURIER SPACE TO VERTICAL VELOCITIES IN
C     REAL SPACE.
C
C
      PARAMETER(NX=64,NY=64,N=52)
      REAL*8 W(128,64),RE(64,64),JUNK(128)
      INTEGER IX,IZ,IY,L
C
C... READ IN VERTICAL VELOCITY FIELD IN FOURIER SPACE
C     CALCULATED IN PROGRAM FOURSP.
C
5     FORMAT(F30.8)
      DO 10 L=1,N
      WRITE (*,*) 'STARTING TRANSFORM',L
      OPEN(7,FILE='RESULTS')
      DO 50 IY=1,NY
```

```
      DO 40 IZ=1,N
      IF (L .EQ. IZ) THEN
      READ(7,5) (W(IX,IY),IX=1,2*NX)
      ELSE
      READ(7,5) (JUNK(IX),IX=1,2*NX)
      ENDIF
40    CONTINUE
50    CONTINUE
C
C...  INVOKE FFT
C
      CALL FOURA(NX,NY,W,RE)
C
C...  WRITE VERTICAL VELOCITY FIELD IN REAL SPACE TO FILE.
C
      OPEN(8,FILE='FINAL')
      WRITE(8,5) ((RE(IX,IY),IX=1,NX),IY=1,NY)
      CLOSE (7)
10    CONTINUE
      END
C
C
C
      SUBROUTINE FOURA(NX,NY,W,RE)
C
C
      REAL*8 WR,WW,WPR,WPI,THETA,W(128,64),TEMPR,WI(64,128)
      REAL*8 WTEMP,TEMPI,RE(64,64)
      INTEGER NX,NY,NN,I,J,NMAX,M,ISIGN,K
C
      ISIGN=-1
      DO 400 Y=1,NY
      NN=2*NX
      J=1
      DO 100 I=1,NN,2
      IF (J.GT.I) THEN
      TEMPR=W(J,Y)
      TEMPI=W(J+1,Y)
      W(J,Y)=W(I,Y)
      W(J+1,Y)=W(I+1,Y)
      W(I,Y)=TEMPR
      W(I+1,Y)=TEMPI
      ENDIF
      M=NN/2
1     IF ((M.GE.2).AND.(J.GT.M)) THEN
      J=J-M
      M=M/2
      GO TO 1
      ENDIF
      J=J+M
```

```
100   CONTINUE
      NMAX=2
2     IF (NN.GT.NMAX) THEN
      ISTEP=2*NMAX
      THETA=6.2831853/(ISIGN*NMAX)
      WPR=-2.D0*DSIN(0.5D0*THETA)**2
      WPI=DSIN(THETA)
      WR=1.D0
      WW=0.D0
      DO 300 M=1,NMAX,2
      DO 200 I=M,NN,ISTEP
      J=I+NMAX
      TEMPR=SNGL(WR)*W(J,Y)-SNGL(WW)*W(J+1,Y)
      TEMPI=SNGL(WR)*W(J+1,Y)+SNGL(WW)*W(J,Y)
      W(J,Y)=W(I,Y)-TEMPR
      W(J+1,Y)=W(I+1,Y)-TEMPI
      W(I,Y)=W(I,Y)+TEMPR
      W(I+1,Y)=W(I+1,Y)+TEMPI
200   CONTINUE
      WTEMP=WR
      WR=WR*WPR-WW*WPI+WR
      WW=WW*WPR+WTEMP*WPI+WW
300   CONTINUE
      NMAX=ISTEP
      GO TO 2
      ENDIF
400   CONTINUE
      DO 410 K=1,NY
      DO 410 P=1,NX*2
      W(P,K)=W(P,K)/FLOAT(NX)
410   CONTINUE
      T=1
      DO 460 Y=1,NY*2,2
      S=1
      DO 470 I=1,NX
      WI(I,Y)=W(S,T)
      WI(I,Y+1)=W(S+1,T)
      S=S+2
470   CONTINUE
      T=T+1
460   CONTINUE
      DO 900 I=1,NX
      NN=2*NY
      J=1
      DO 500 Y=1,NN,2
      IF (J.GT.Y) THEN
      TEMPR=WI(I,J)
      TEMPI=WI(I,J+1)
      WI(I,J)=WI(I,Y)
      WI(I,J+1)=WI(I,Y+1)
```

```
      W(I,Y)=TEMPR
      W(I,Y+1)=TEMPI
      ENDIF
      M=NN/2
3     IF ((M.GE.2).AND.(J.GT.M)) THEN
      J=J-M
      M=M/2
      GO TO 3
      ENDIF
      J=J+M
500   CONTINUE
      NMAX=2
4     IF (NN.GT.NMAX) THEN
      ISTEP=2*NMAX
      THETA=6.2831853/(ISIGN*NMAX)
      WPR=-2.D0*DSIN(0.5D0*THETA)**2
      WPI=DSIN(THETA)
      WR=1.D0
      WW=0.D0
      DO 700 M=1,NMAX,2
      DO 600 Y=M,NN,ISTEP
      J=Y+NMAX
      TEMPR=SNGL(WR)*WI(I,J)-SNGL(WW)*WI(I,J+1)
      TEMPI=SNGL(WR)*WI(I,J+1)+SNGL(WW)*WI(I,J)
      WI(I,J)=WI(I,Y)-TEMPR
      WI(I,J+1)=WI(I,Y+1)-TEMPI
      WI(I,Y)=WI(I,Y)+TEMPR
      WI(I,Y+1)=WI(I,Y+1)+TEMPI
600   CONTINUE
      WTEMP=WR
      WR=WR*WPR-WW*WPI+WR
      WW=WW*WPR+WTEMP*WPI+WW
700   CONTINUE
      NMAX=ISTEP
      GO TO 4
      ENDIF
900   CONTINUE
      DO 910 K=1,NY*2
      DO 910 P=1,NX
      WI(P,K)=WI(P,K)/FLOAT(NY)
910   CONTINUE
      J=1
      DO 920 K=1,NY*2,2
      DO 915 I=1,NX
      RE(I,J)=WI(I,K)
915   CONTINUE
      J=J+1
920   CONTINUE
      RETURN
      END
```